

ESD ACCESSION LIST

XNRI Call No. 82849

Copy No. 1 of 2 cys.

Technical Note

1975-22

M. L. Burrows

Strain-Gage Vibration Measurements
on a Submarine-Towed Antenna Cable

27 May 1975

Prepared for the Department of the Navy
under Electronic Systems Division Contract F19628-73-C-0002 by

Lincoln Laboratory

MASSACHUSETTS INSTITUTE OF TECHNOLOGY

LEXINGTON, MASSACHUSETTS



Approved for public release; distribution unlimited.

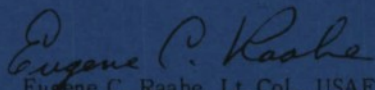
ADA012287

The work reported in this document was performed at Lincoln Laboratory, a center for research operated by Massachusetts Institute of Technology. The work was sponsored by the Department of the Navy under Air Force Contract F19628-73-C-0002.

This report may be reproduced to satisfy needs of U.S. Government agencies.

This technical report has been reviewed and is approved for publication.

FOR THE COMMANDER

A handwritten signature in dark ink, reading "Eugene C. Raabe". The signature is written in a cursive style with a large, stylized "E" and "R".

Eugene C. Raabe, Lt. Col., USAF
Chief, ESD Lincoln Laboratory Project Office

MASSACHUSETTS INSTITUTE OF TECHNOLOGY
LINCOLN LABORATORY

STRAIN-GAGE VIBRATION MEASUREMENTS
ON A SUBMARINE-TOWED ANTENNA CABLE

M. L. BURROWS

Group 61

TECHNICAL NOTE 1975-22

27 MAY 1975

Approved for public release; distribution unlimited.

LEXINGTON

MASSACHUSETTS

ABSTRACT

As part of the work on the development of a submarine-towed ELF loop antenna, the mechanics of cable vibration have been studied both analytically and experimentally. In particular, measurements of towed cable vibrations have been carried out from surface vessels and from a submarine. This note presents the results of these measurements, which, after some preliminary accelerometer measurements, were obtained with a buoyant cable equipped with strain gages.

The results are that both cable longitudinal strain and cable curvature, over the frequency range of 20 to 200 Hz, are excited by the fluctuating forces on the surface of the cable arising from the cable's own turbulent boundary layer. Neither vibration of the tow point nor the submarine wake are significant sources of mechanical energy. Generalized force spectra are derived from the measured vibration spectra. These then allow the levels of both types of vibration to be calculated for an arbitrary cable towed at an arbitrary speed.

CONTENTS

Abstract	iii
I. Introduction	1
II. Accelerometer Measurements	2
III. Strain-Gage Measurements	17
IV. Derived Force Spectra	37
V. Conclusions	43
Appendix A - Strain-Gage Pair Data Processing	45
References	57

Strain-Gage Vibration Measurements on a Submarine-Towed Antenna Cable

I. Introduction

This report describes the results of strain-gage measurements, made in 1972, of the vibration of a submarine-towed antenna cable. These measurements, taken together with some preliminary measurements made on a cable fitted with an accelerometer array, have played a decisive role in the analysis of towed antenna noise and in the development of techniques to overcome it [1,2,3,4,5].

The significance of knowing how and why the cable vibrates can be illustrated by the following questions:

i) How long should the tail be? (The tail is the electrically inactive length of cable, aft of the antenna section, and used to isolate the antenna from any end instabilities.)

ii) Will it help to place mechanical isolators in the cable to prevent vibrational energy propagating along the cable from tail or tow point into the antenna region?

iii) Would the use of a longer antenna cable help? The longer cable would place the antenna region of the cable further away from the large wake eddies of the submarine.

iv) Is the cable vibration the only significant source of the noise induced by towing the antenna, or is hydromagnetic noise a factor? Hydromagnetic noise is the noise voltage induced in the antenna by the electrical currents in the surrounding water. These currents, in turn, are produced by the turbulent motion of the electrically conductive sea water in the geomagnetic field.

The next section describes briefly the results of accelerometer measurements, which provided invaluable experimental support in the evolution of the theory of vibrational wave propagation along the towed cable. However, the accelerometer installation unavoidably so modified the cable diameter and mechanical properties that it could not pass out through the deployment mech-

anism of a submarine and would not, in any case, give an accurate measure of the vibration level of an unmodified cable. The measurements were therefore carried out from a surface boat using a depressor (a device like an upside down kite) to lower the tow point to the appropriate depth.

The basic quantitative vibration data for an unmodified cable towed behind a submarine were obtained with strain gages. These measurements are described in Section III and the results are digested and summarized in Section IV.

II. Accelerometer Measurements

The accelerometer experiment was carried out as a joint venture by the Navy Underwater Systems Center, New London Laboratory and Lincoln Laboratory. The latter designed the experiment and directed the data processing. The former was responsible for installing the accelerometers, for providing the instrumentation and for carrying out the data processing.

A total of seven accelerometers were installed, an array of five to measure transverse accelerations in a common plane at five different points within a total distance of 3.4m, one to measure the transverse acceleration in the perpendicular direction and one to measure in the longitudinal direction (see Fig. 1). The towing configuration is shown in Fig. 2.

The accelerometer signals were recorded on magnetic tape, digitized and then processed in pairs to obtain the individual auto spectra, the cross spectrum, the coherence function, the transfer function and the impulse response.

In the first experimental run, the most striking feature in the result of processing between pairs in the array of five was the disclosure that the

18-6-16514

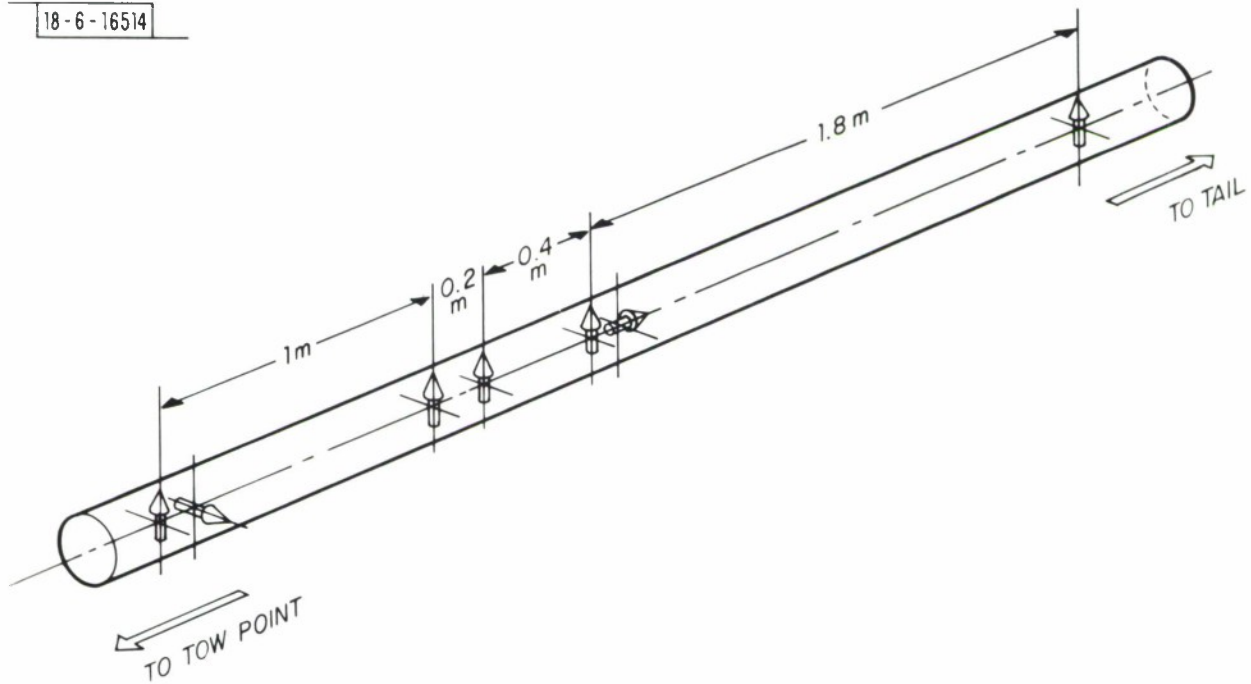


Fig. 1. The placing and orientation of the seven accelerometers in the cable.

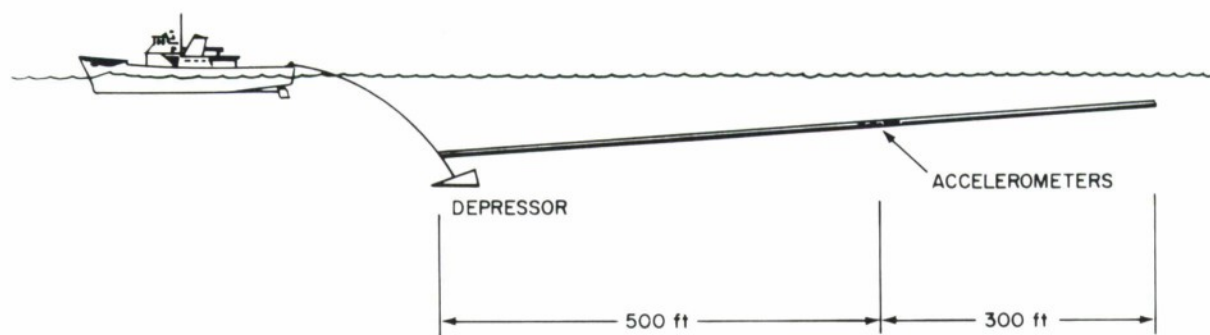


Fig. 2. The towing configuration of the boat, depressor and cable.

transverse waves were propagating in one direction only--towards the tow point. Figure 3 shows, for example, the impulse response between the two accelerometers 3.4m apart. If the cable vibration had had transverse waves of comparable amplitude traveling in both directions, there would be a structure on the right side of the time origin mirroring that developed very clearly on the left.

The shape of the impulse response is that expected for a dispersive transmission line. The wave velocity and attenuation are greater at higher frequencies, due to the effect of cable stiffness, so that the smaller amplitude higher frequency waves arrive first.

The phase response is shown in Fig. 4, and this again gives strong evidence of the unidirectional propagation, for the phase is a monotonically increasing function of frequency. It can be used as a check on the stiff taut string model of the mechanical properties of the cable, which expresses the relationship between the wave number of the propagating wave and the ratios stiffness over mass and tension over mass [2]. In Fig. 5, the plotted points were obtained by noting the frequencies at which successive half-cycle increments in phase occur in Fig. 4. The continuous line is the phase difference predicted by the stiff taut string model using the parameter values shown. Thus the general form of the propagation seems to be well described by the stiff taut string model.

It should be noted that the accelerometer installation caused a very marked stiffening of the cable and that the tail end of the cable tangled into a large knot, which was not noticed until the cable was being retrieved, and

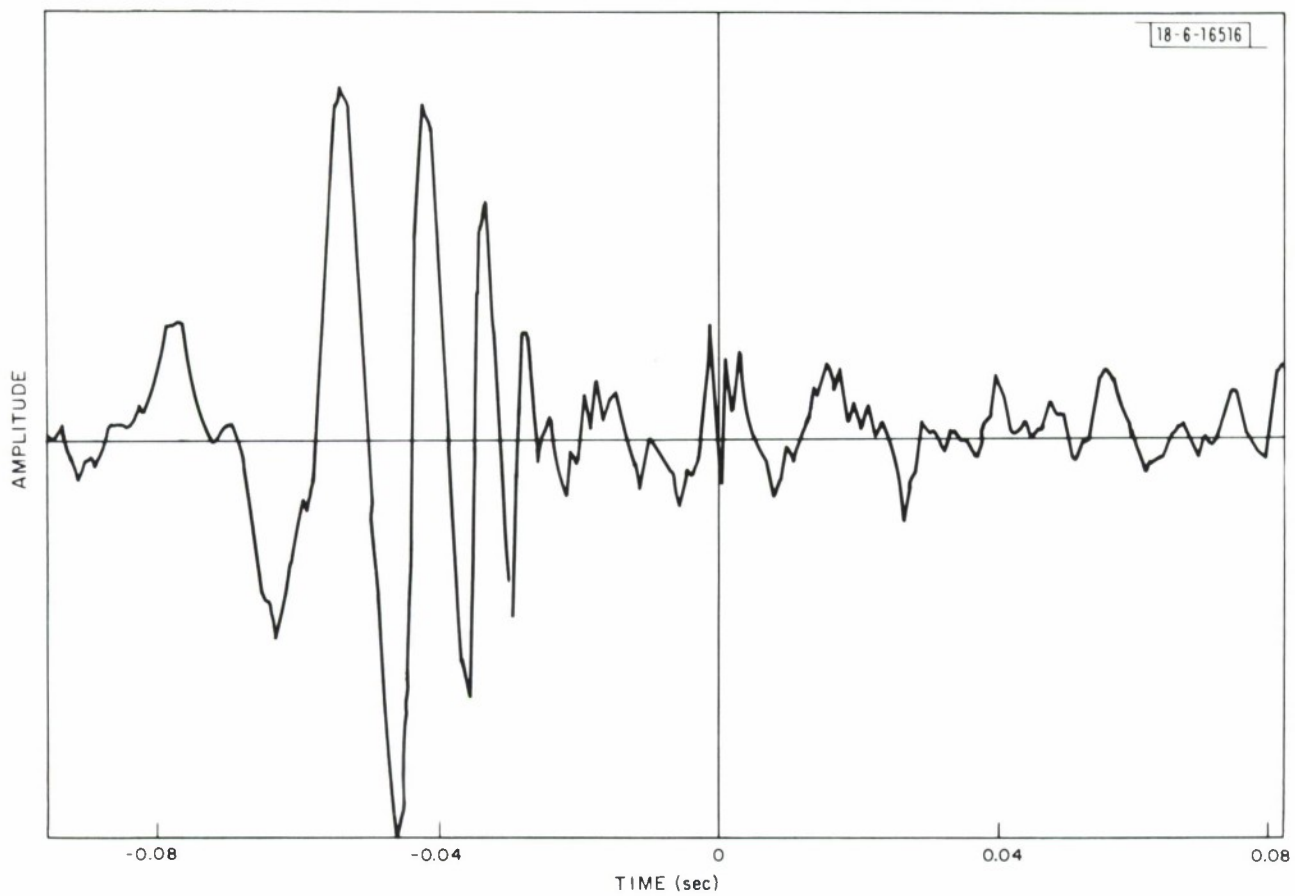


Fig. 3. The impulse response between the two accelerometers 3.4 m apart in the array of five.

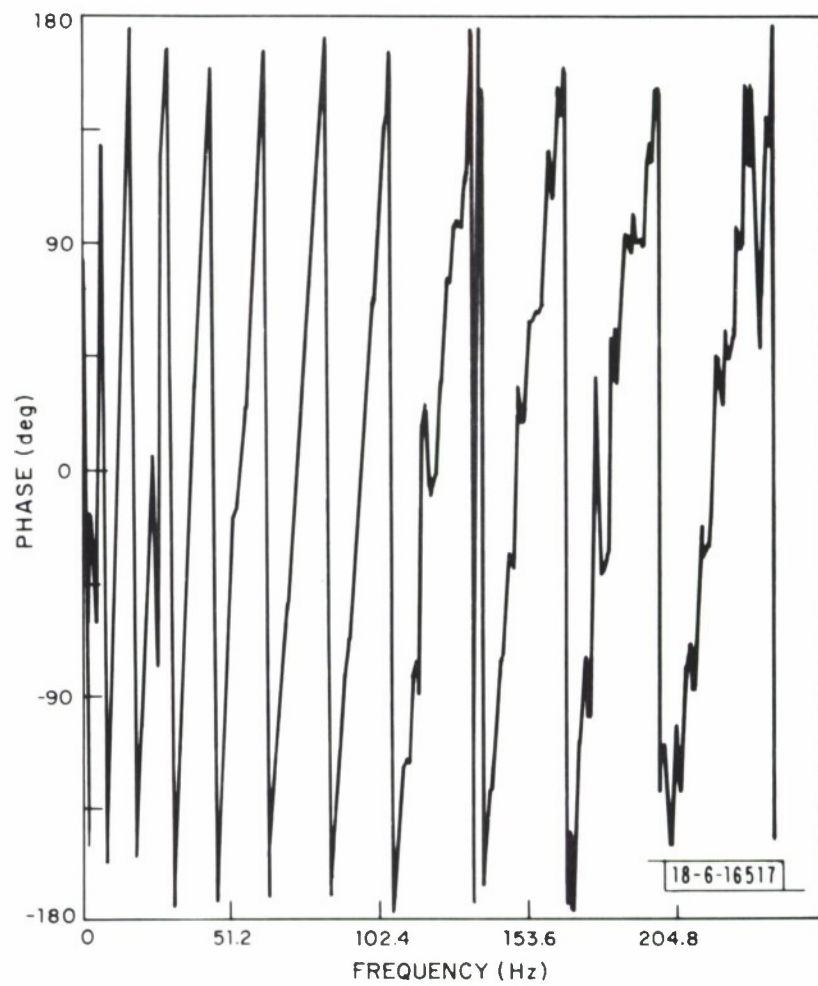


Fig. 4. The phase response between the two accelerometers 3.4 m apart in the array of five.

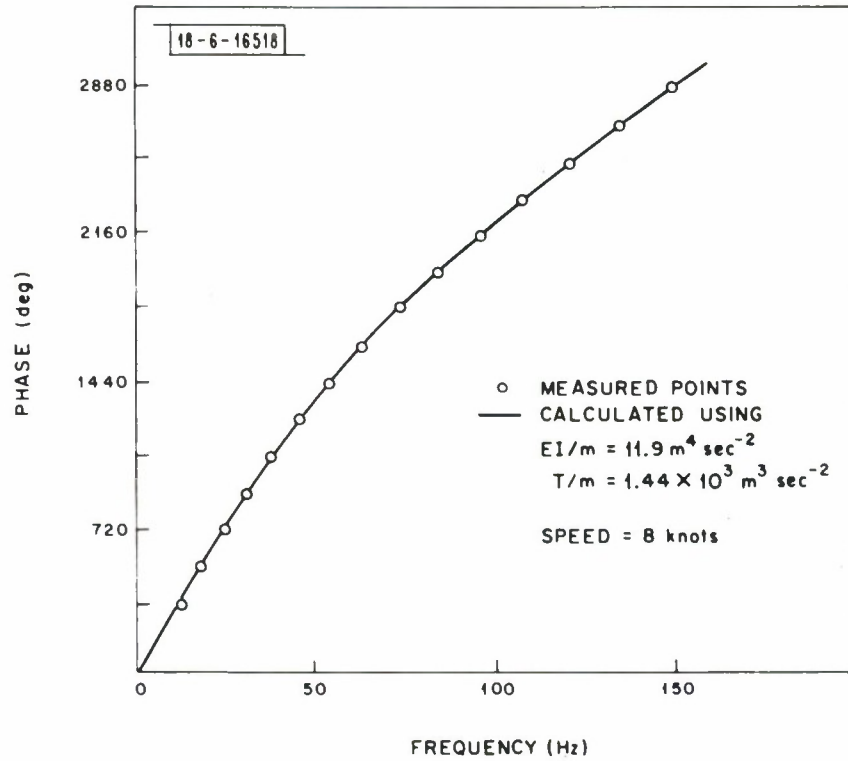


Fig. 5. Phase difference, for transverse wave propagation over a distance of 3.4 m, versus frequency.

which would make the tension larger than expected. It is not surprising, therefore, that the parameter values used to make the curve fit the measured data are larger than those obtained from direct measurement of the physical properties of the cable, which are $3.4 \text{ m}^4 \text{ sec}^{-2}$ for EI/m and $0.62 \times 10^3 \text{ m}^2 \text{ sec}^{-2}$ for T/m .

Other results of this first run were that the coherence between mutually orthogonal pairs of accelerometers was in all cases too small to measure, indicating that the vibrations in the three principal directions are statistically independent. In addition, the output levels of all transverse sensors remained constant in time, which indicates that the transverse vibration was statistically isotropic. For if it were not, then the sensors would have shown a signal level variation due to cable rotation.

For this first test, the 300 ft. tail section was mechanically fastened to the rest of the cable with a braided metal sleeve clamped to each cable piece with two standard hose clamps. The clamps were located about five feet aft of the last sensor. It was suspected that the protruding tightening screw on each clamp, which generated hydrodynamic disturbances in the water and was in turn buffeted by them, was the source of the cable vibrations. Their direction of energy flow was certainly consistent with this view.

For subsequent tests, therefore, the tail was reconnected using a smoothly faired connector. The results were i) the level of the vibration dropped, ii) the phase and cross-spectrum taken between pairs of accelerometers showed the features characteristic of essentially equal amplitude uncorrelated energy flow in both directions, iii) shortening the tail by 100 ft. caused a

slight reduction in the level of the vibration but left the symmetry of the energy flow unchanged. Thus, in view of the large attenuation of transverse waves [2], the mechanical energy must arise locally, for otherwise the symmetry of the energy flow would have been profoundly changed by what was, in effect, a change in the location of the array of 100 ft. In addition, the view that the hose clamps were the source of the vibration measured in the first test was shown to be true.

The phase plots between the same two accelerometers for the first run and for the second run at both tail lengths are shown in Figs. 6, 7 and 8. Clearly marked is the difference between the smooth phase progression of the first and the progression by jumps of the other two. The corresponding cross-spectra are shown in Figs. 9, 10 and 11. Again the difference between the first, which show the characteristic periodicity, is clearly marked. The minima in the cross-spectra coincide with the phase jumps in the corresponding phase plots, as expected.

No longitudinal acceleration data are reported here because the attenuation of longitudinal waves in the cable is small [2]. This allows disturbances generated at the depressor to travel along to the accelerometer location and dominate other sources of longitudinal strain energy there. Also, since only one longitudinally oriented accelerometer was used, no longitudinal wave structure analysis, like that carried out for transverse waves between pairs of transversely oriented accelerometers, was possible.

The outcome of the accelerometer measurements was, then, that the two orthogonal directions of the transverse vibration and the longitudinal vibra-

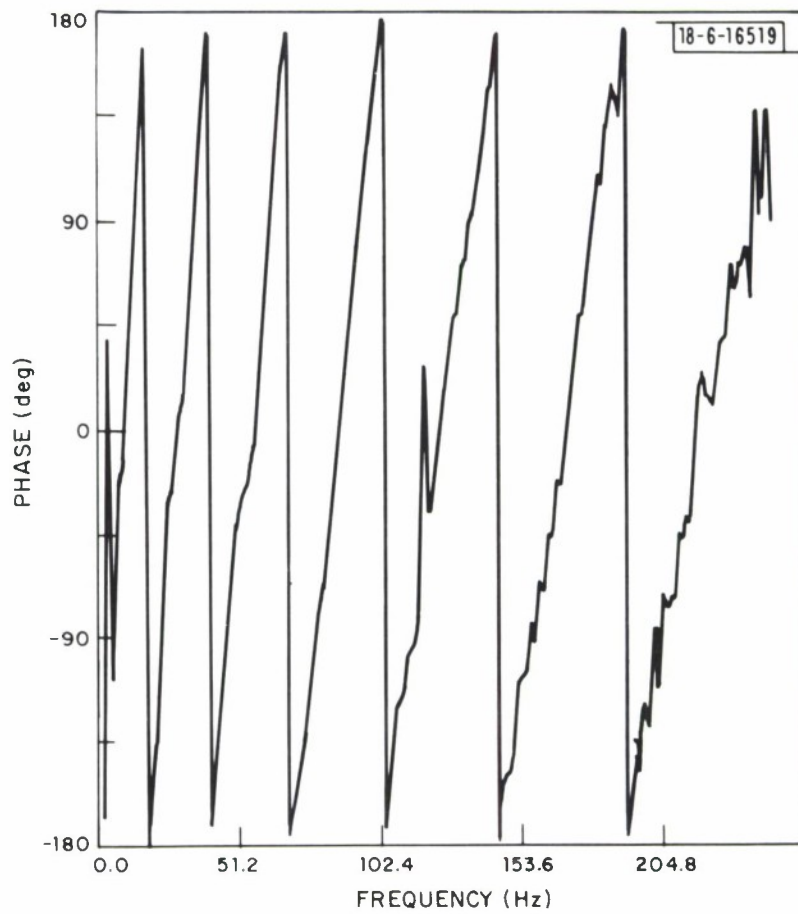


Fig. 6. Phase response at 2.2 m spacing and 8 knots with a 300 ft. tail and hose clamps present.

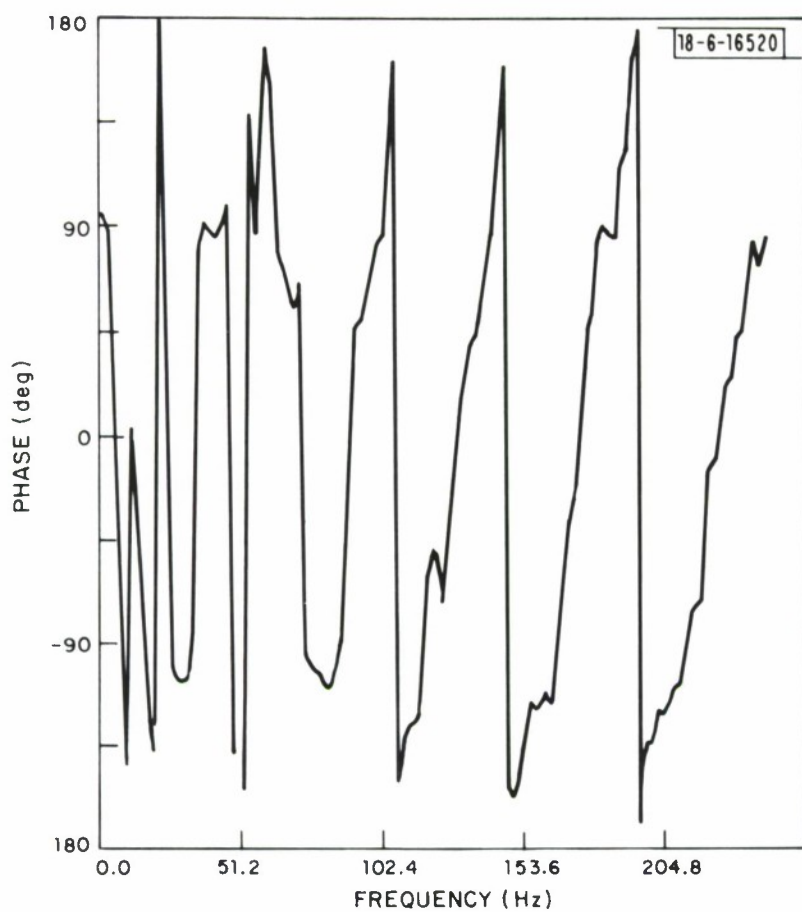


Fig. 7. Phase response at 2.2 m spacing and 8 knots with a 300 ft. tail and no hose clamps present.

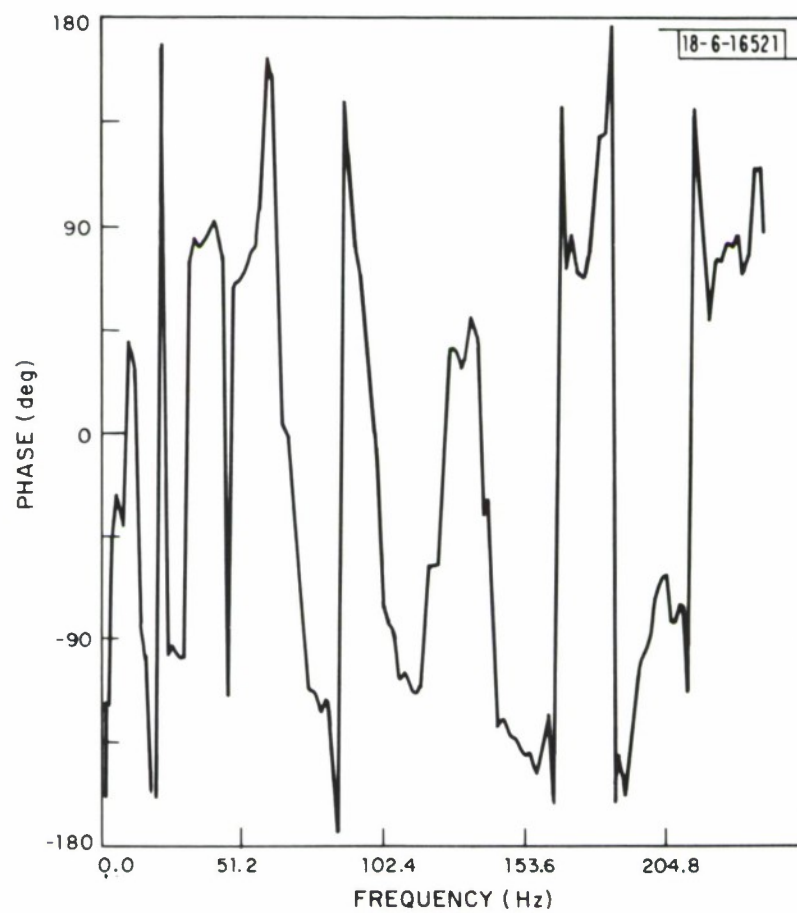


Fig. 8. Phase response at 2.2 m spacing and 8 knots with a 200 ft. tail and no hose clamps present.

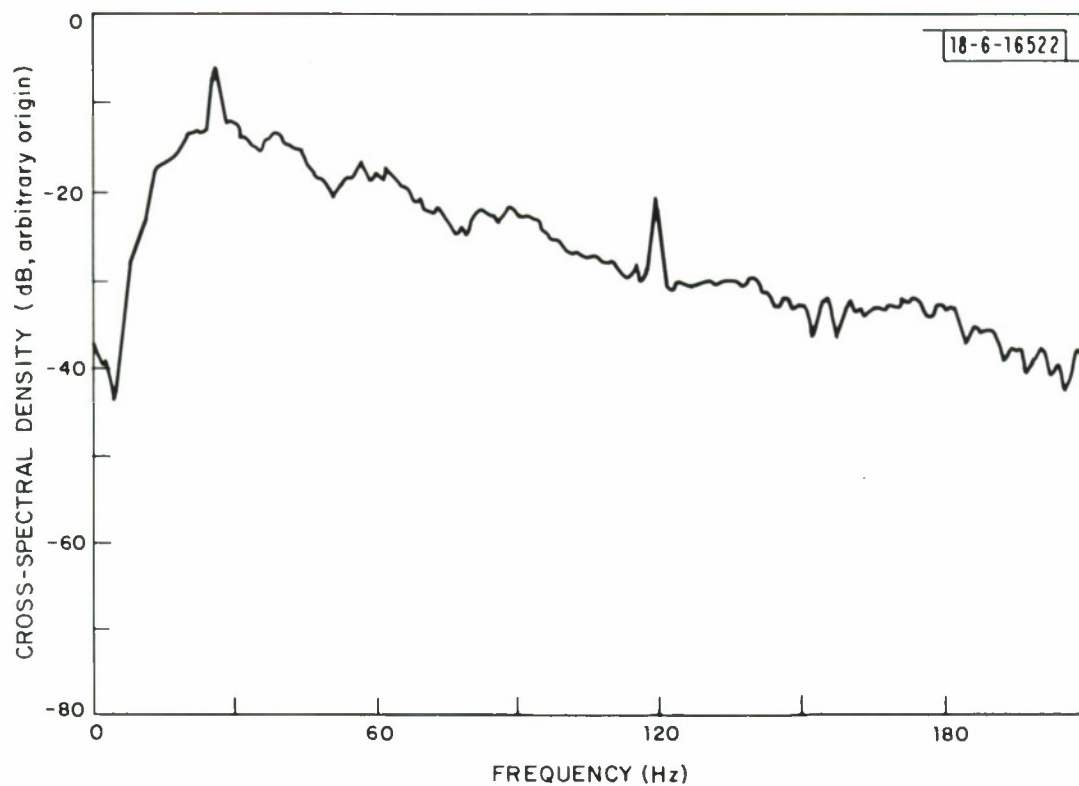


Fig. 9. Cross-spectrum at 2.2 m spacing and 8 knots with a 300 ft. tail and hose clamps present.

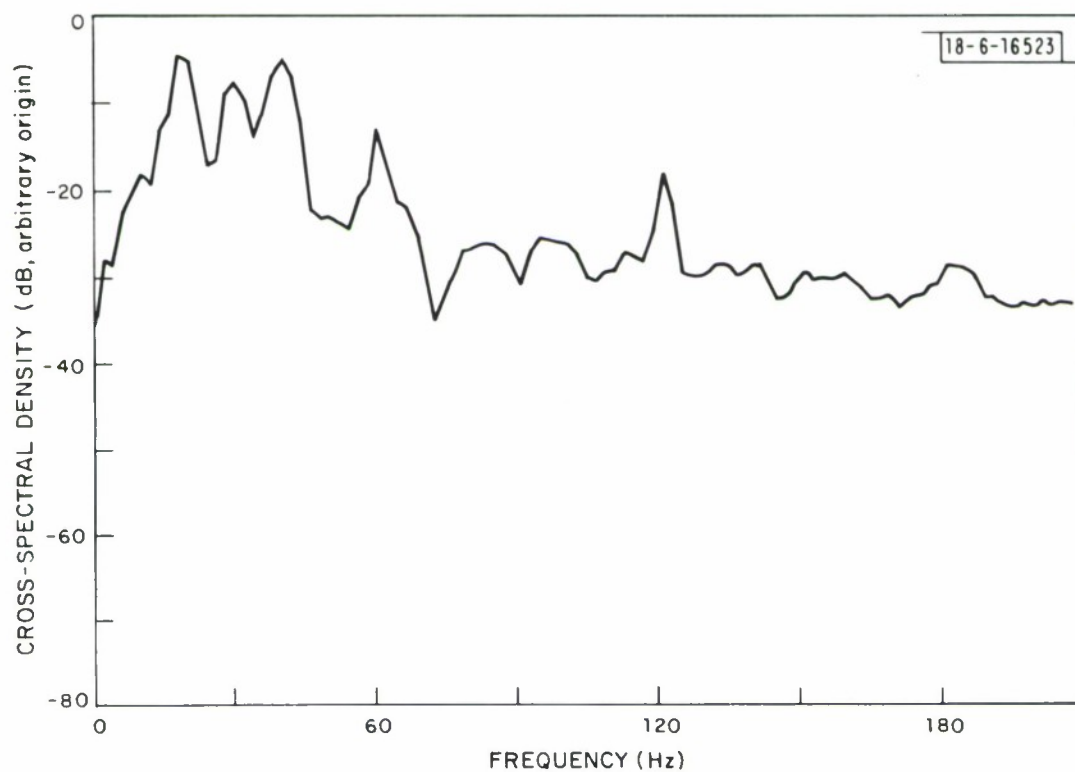


Fig. 10. Cross-spectrum at 2.2 m spacing and 8 knots with a 300 ft. tail and no hose clamps present.

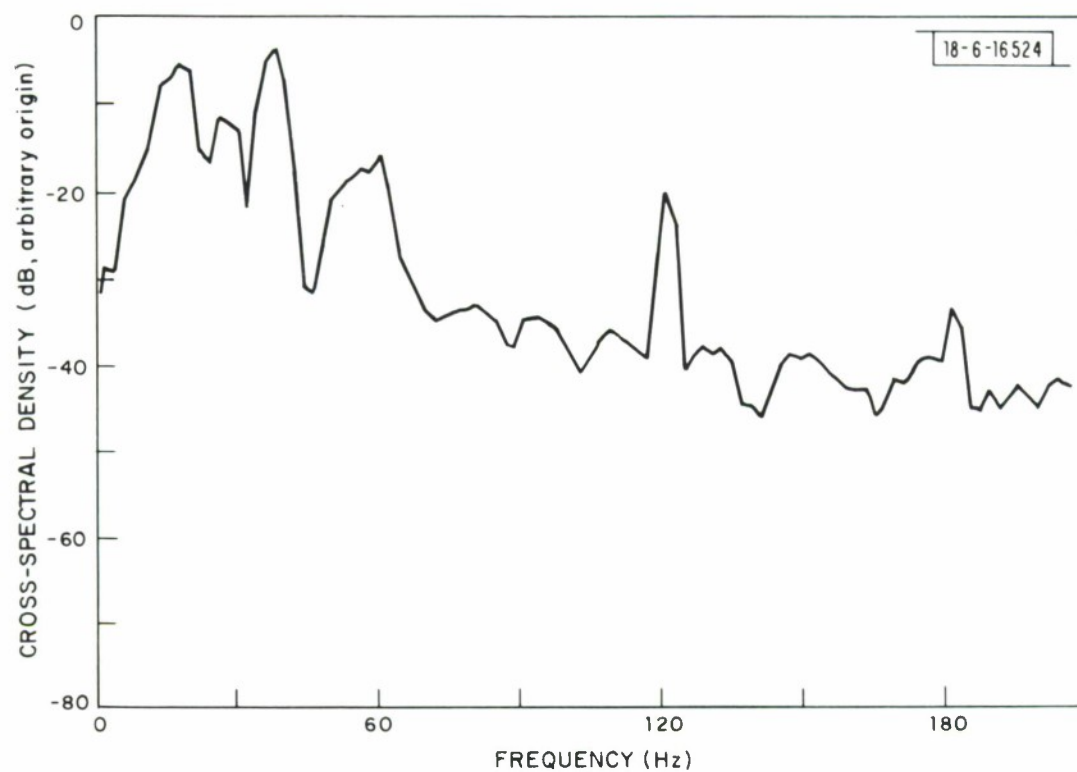


Fig. 11. Cross-spectrum at 2.2 m spacing and 8 knots with a 200 ft. tail and no hose clamps present.

tion are all statistically independent from one another, that the propagation of transverse vibrational waves along the cable is well described by the stiff taut string mathematical model and that the transverse vibration originates neither at the tail end nor at the tow end but is locally generated. Whether the boat wake or the turbulent boundary layer of the cable itself provides the disturbing transverse force cannot be decided from these measurements.

III. Strain-Gage Measurements

The strain gage installation was intended to provide a means for measuring the longitudinal and transverse vibration of the cable separately and at the same time leave the mechanical properties and dimensions of the cable unchanged. The installation and instrumentation have already been described by Nackoney [6]. Briefly, there are six gages installed as three pairs at three locations in a 2000 ft. long, 14 conductor buoyant cable (Fig. 12a). The two gages in each pair are emplaced diametrically opposite one another in the buoyant cable jacket and have their sensitive axes parallel to the cable axis (Fig. 12b). The sum of the strains registered by each member of the gage pair is a measure of the longitudinal strain of the cable at the gage-pair location. The difference between the strains is a measure of the curvature of the cable axis at the same location.

If the gages are perfectly matched and the installation is both geometrically and mechanically perfectly symmetrical, the strain sum should be independent of the cable curvature and the strain difference should be independent of the cable longitudinal strain. But the gages are not perfectly matched, the cable is not perfectly symmetrical and the installation procedure is imper-

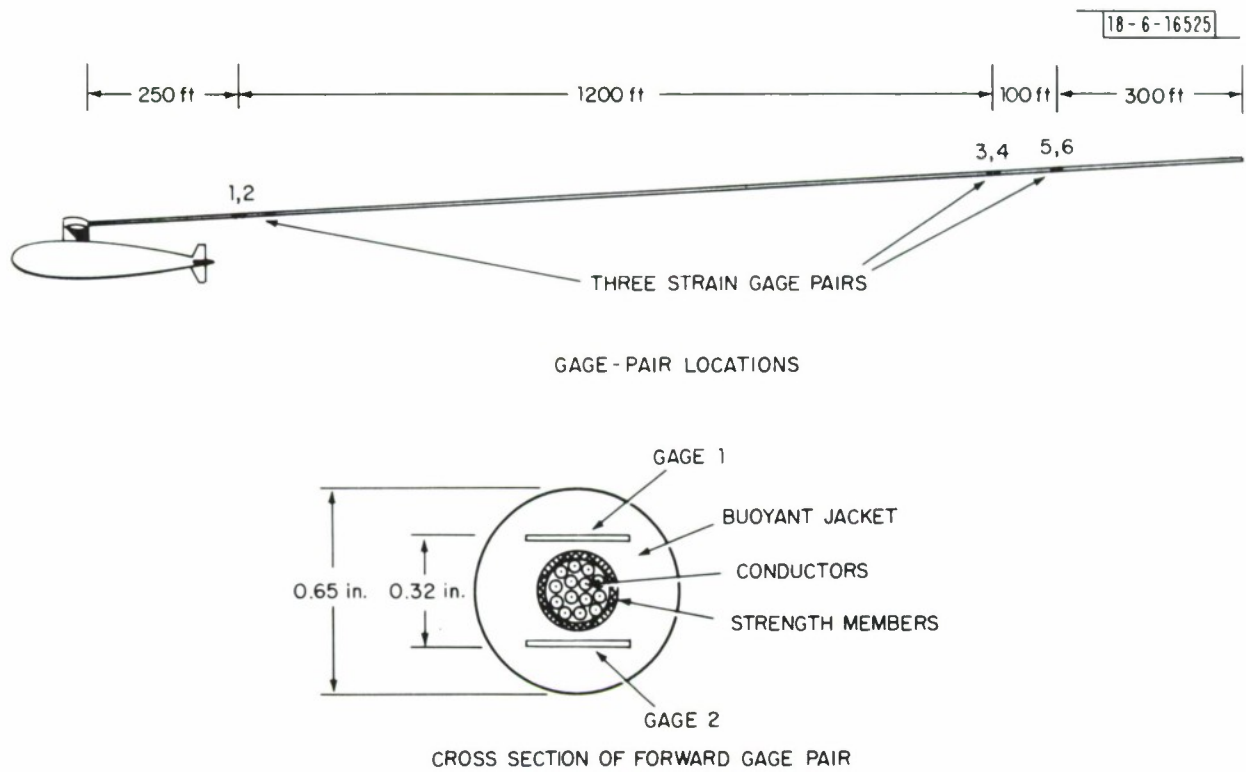


Fig. 12. Strain gage experiment showing gage-pair location and the gage placement in the cable cross section.

fect. So the question arises of how the gain of the amplifier serving each member of a gage pair is to be determined to reject the unwanted signal. This question is particularly critical if the curvature signal, for example, is very much larger than the longitudinal strain signal. For then, a slight error in gain setting in forming the strain sum could lead to enough of the curvature signal left uncanceled to obliterate the required longitudinal strain signal. It is also clear, that, due to differences in gain and phase of the two amplifiers, the proper gain setting could well be a complex number which is a function of frequency.

Fortunately, the longitudinal and transverse vibrations of the cable can be assumed to be statistically independent. Such an assumption was shown experimentally to be valid for the accelerometer array cable. It is shown in the Appendix that this simple assumption makes it possible to define a method of data processing which establishes the proper gain setting, as a function of frequency, in phase and amplitude, by means of certain averages performed on the two strain signals. This gain adjustment, and its application to calculate the separate longitudinal strain and curvature spectra, was carried out in a digital computer. The input to the computer was the two separate digitized and synchronized strain signals. Its output was the separate required spectra.

The first test of the strain gage cable was carried out on the surface. It served as a dress rehearsal for the submarine test to follow. No depressor was used, so the cable simply floated along the surface behind the towing boat. The test was successful in demonstrating that the whole system--cable,

instrumentation and recording--functioned properly. It was uneventful except for a valuable corroboration of the theory for longitudinal strain wave propagation along the cable.

Figure 13 shows short (c. 4.5 sec) simultaneous samples of the sum strain from each gage pair. These were obtained by using summing amplifiers rather than the digital process described in the Appendix (which can produce only spectral averages). Each amplifier's gain balance setting was determined solely by the criterion that the gain in all channels be the same.

The strain signals show very strong correlation from pair to pair with a delay equivalent to a speed of about 6×10^3 ft./sec apparent between the tow-point pair and the tail mounted pairs. The tail pair signals are of smaller magnitude than the tow-point ones. Thus, for the dominant frequency components visible here and for this surface test of the cable, one concludes that the longitudinal strain energy was generated near the tow point and then propagated towards the tail.

Figure 14 shows the corresponding simultaneous samples of the difference strain from each gage pair. These signals are proportional to the local curvature of the cable. There is no visually apparent correlation from pair to pair and the curvature variation increases in magnitude towards the tail. This suggests that the curvature (and therefore also the transverse vibration) was locally generated, for this surface test.

The submarine test consisted of towing the strain gage cable at various speeds in straight runs for three different cable configurations, executing a continuous heading change (i.e., a circular turn) at various speeds and

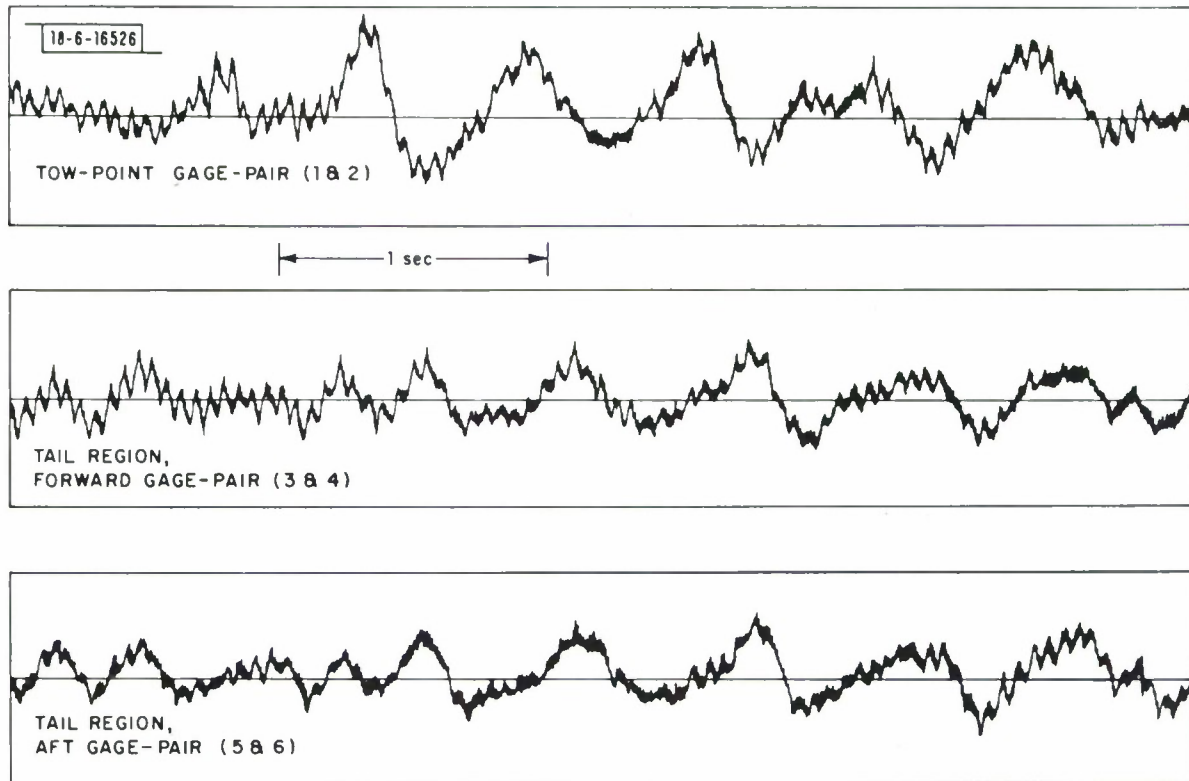


Fig. 13. Simultaneous longitudinal strain signals from the three gage pairs at a speed of 8 knots on the surface.

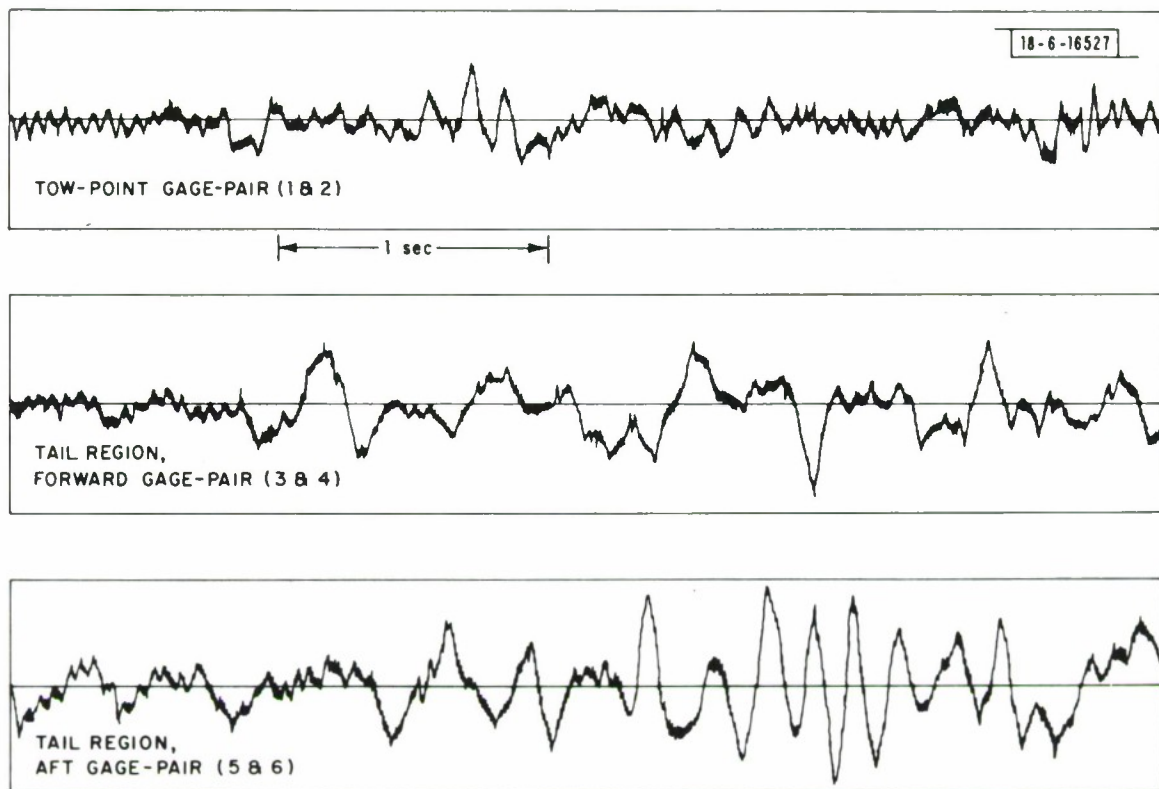


Fig. 14 Simultaneous curvature signals for the three gage pairs at a speed of 8 knots on the surface.

performing a slow speed-increase run. For each run, the strain signals from the six gages were recorded separately on six channels of a magnetic tape recorder. After the test, the signals were digitized and processed as described in the Appendix.

The three different cable configurations used in the straight runs were, first, with 1850 ft. of cable being towed as shown in Fig. 12; second, with only 1150 ft. of cable being towed and, third, after 200 ft. had been cut off the tail end, with 1650 ft. of cable being towed. For the turns and for the slow speed increase runs, the cable configuration used was the first (1850 ft. total tow length, 300 ft. from tail end to gages 5 and 6).

The story told by the longitudinal strain results was that the longitudinal strain spectrum is largely the same at all gage pair stations for both the long scope straight runs (1650 ft. and 1850 ft. of cable towed) and the short scope straight run (1150 ft. of cable towed). Figure 15 shows the longitudinal strain spectra at 12 knots from a total of eight gage pair locations superimposed on one another. The locations were 1600 ft., 400 ft. and 300 ft. from the tail end with 1850 ft. of cable towed; 1400 ft., 200 ft and 100 ft. from the tail end with 1650 ft. of cable towed; and 400 ft. and 300 ft. from the tail end with 1150 ft. of cable towed. It can be seen that all spectra lie very close to one another. For practical purposes, therefore, they can be represented by a single spectrum.

This suggests that the longitudinal strain energy in the cable is supplied locally, with the cable's own turbulent boundary layer being the prime candidate for the source, rather than a vibrating tow point or the strong turbu-

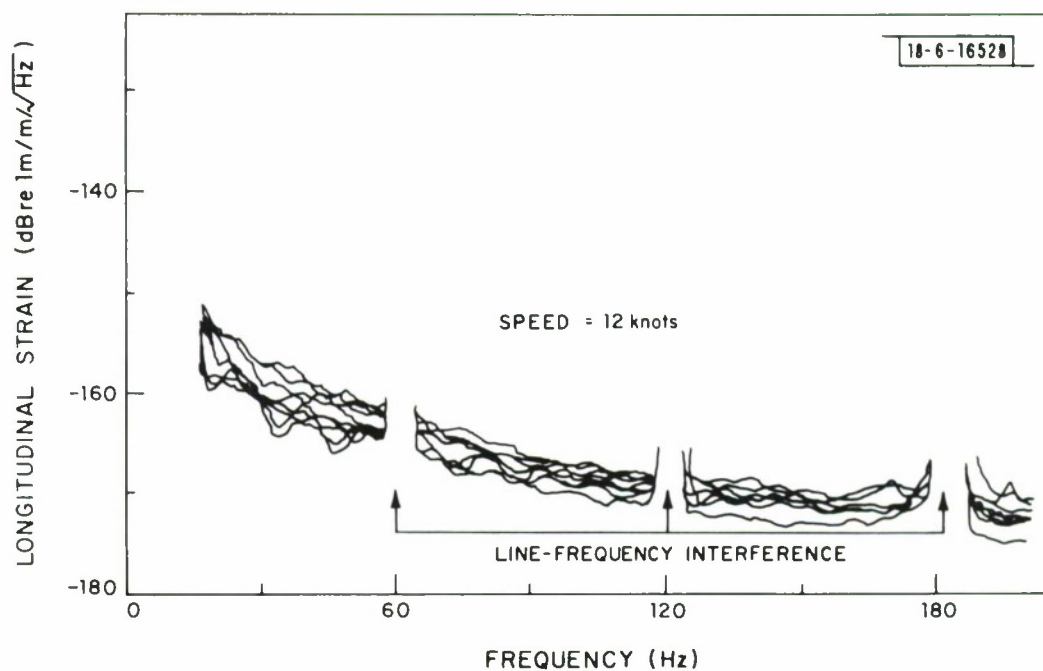


Fig. 15. Longitudinal strain spectra at 12 knots at gage-pairs located 100, 200, 300, 400, 1400 and 1600 feet from the tail end.

lence in the immediate vicinity of the submarine. This point of view is very well corroborated by the detailed structure of the spectrum at the forward gage pair. Two such spectra are cluttered up with six others in Fig. 15, but one of them is shown alone in Fig. 16.

The structure of interest here is the sequence of regularly spaced maxima and minima in the spectrum. By projecting the sequence back to the origin, one finds that a maximum would occur there. This fits a standing wave model in which the strain is proportional to $\sin(k_\ell z)$, where z is the distance from the tow point and k_ℓ is the longitudinal strain wave number. Since $k_\ell = \omega/c_\ell$, where c_ℓ is the longitudinal strain wave velocity, the model predicts that a strain maximum occurs when $\omega = 0$.

The model also predicts that the minima should have a constant spacing Δf given by $2\pi\Delta f z/c_\ell = \pi$. Thus, from the spacing of about 26.5 Hz shown in Fig. 16, and from the value of 76 m (250 ft.) for z , the wave speed c_ℓ works out to be 2170 m/sec. But c_ℓ can also be calculated from the cable longitudinal stiffness EA and its effective mass per unit length m_ℓ . Then $c_\ell = \sqrt{EA/m_\ell}$. The measured value of EA (see Section IV) is $0.9 \times 10^6 \text{ N}$ and the cable specific gravity is about 0.75, so c_ℓ turns out to be 2050 m/sec by this method. The close agreement between the two speed calculations leads one to conclude that the regular structure of the spectrum arises from the wave interference, at the location of the gage pair, between the strain energy propagating along the cable towards the tow point and the same energy being reflected at the tow point and propagating back the other way.

If the source of the strain energy on the cable were a vibrating tow

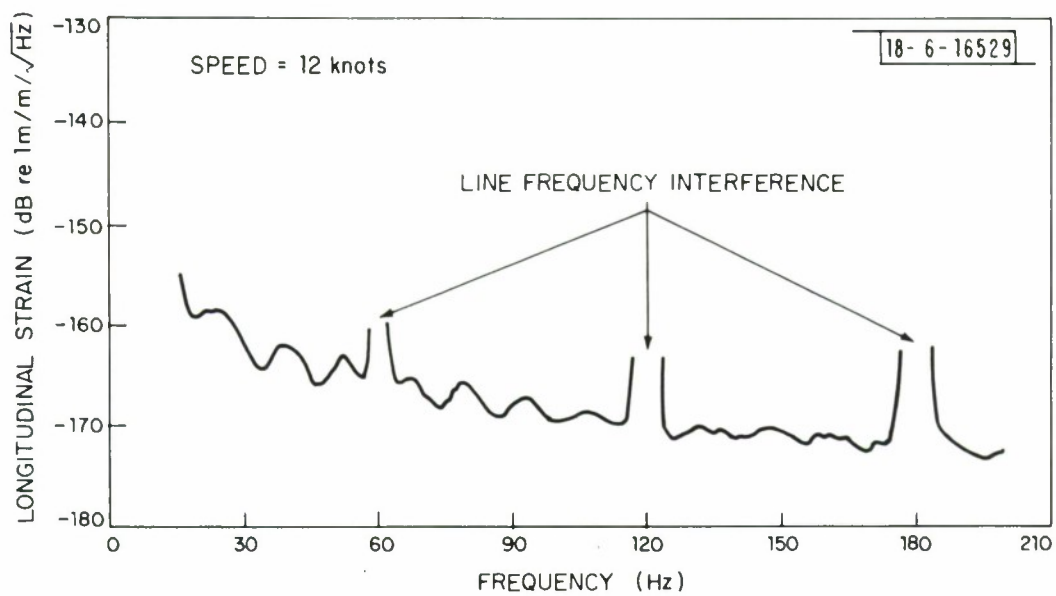


Fig. 16. Longitudinal strain spectrum at 12 knots at the forward gage-pair (1600 ft. from the tail end, 250 ft. from the tow point).

point, the energy would tend to flow only in one direction, towards the tail. The effect of reflections at the tail would not be readily observable at the forward gage pair because of the attenuation involved in traveling practically the whole length of the cable in both directions. This attenuation, at 45 Hz for example, is about 20 dB. Thus the interference effect would be absent.

The characteristics discussed above and depicted in Figs. 15 and 16 apply equally well at the other speeds used. That is, that the strain spectrum is independent of position along the cable and derives its energy of excitation from the cable's own turbulent boundary layer. By drawing a single smoothed average spectrum through the eight spectra shown in Fig. 15, and repeating this for the other speeds the smoothed average curves shown in Fig. 17 were obtained. These show the spectral density of the longitudinal cable strain as a function of speed and frequency.

It should be noted that these strain spectra have been derived from the strain gage signals using a measured value for the gage calibration. The strain spectrum plotted in Ref. 2, and used there to calculate the magnetostrictive noise voltage spectrum in a certain antenna, was based on a calculated gage calibration. The measured calibration was obtained by mechanically exciting the section of cable including each gage pair with a known alternating longitudinal strain and measuring the resulting gage amplifier output voltages. The calculated calibration, on the other hand, simply assumed that the gage behaved like the ideally limp gage which strains the same amount as the surrounding medium without constraining it in any way. The measured calibration resulted in a value of 8 dB re. 1V/unit strain, whereas the calcu-

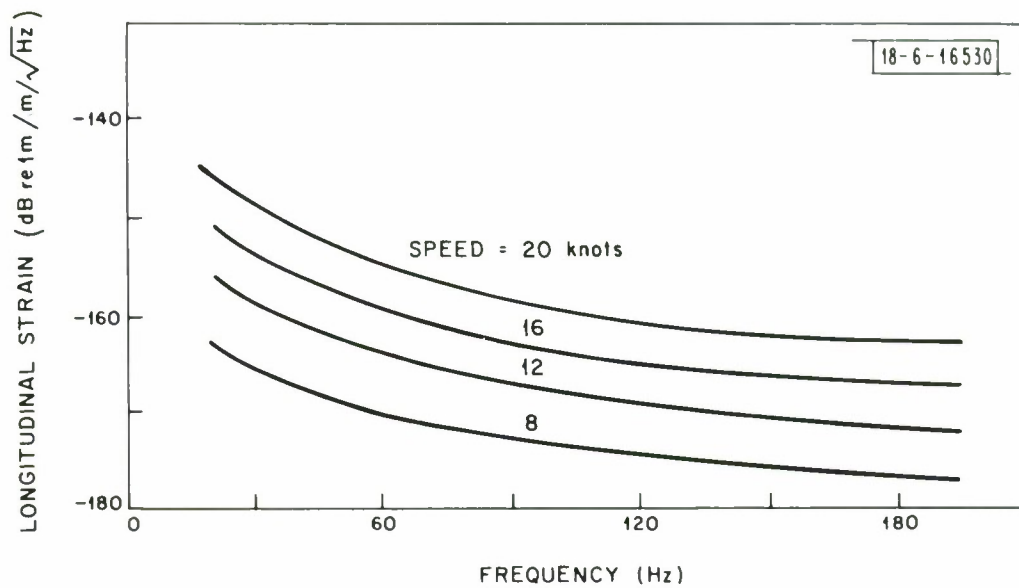


Fig. 17. Smoothed average longitudinal strain spectra at various speeds. The longitudinal strain spectrum is essentially independent of position along the cable except for an interference effect observed near each end.

lated calibration was 14 dB re. 1V/unit strain. That is, the gage, together with its mount, is sufficiently stiff, compared with the soft polymeric jacket in which it is imbedded, for the gage strain to be only half that of the cable itself. This means that the strain spectrum in Fig. 13 of Ref. 2, and the corresponding voltage spectrum, should be raised 6 dB.

If the longitudinal strain, with its long wavelength and low attenuation per unit length, is explained by a local generation model, then the transverse vibration, with its short wavelength and high attenuation per unit length, would be expected certainly to be. The results of the test support this expectation. Figure 18 shows the curvature spectra at five different locations along the cable. (The spectrum for the 300 ft. location is omitted because it lies more or less directly on top of that for 200 ft.) At high frequencies, where the cable's wave properties are determined by the cable stiffness rather than its tension, the spectra all merge into one. At low frequencies this does not occur, because there the tension, which changes continuously over the length of the cable, becomes predominant. Whether the local generation model fits well at the lower frequencies can be examined only by using the cable's mechanical properties (at the location of each gage pair and at each speed) to deduce the driving force spectrum $S_f(0, \omega)$ from the cable response (the curvature spectra). This will be done in the next section for all the testing speeds.

Before leaving this section, however, it is necessary to discuss the results of the circular turn test runs, the slow speed-increase test run and the two-wire gage connection test.

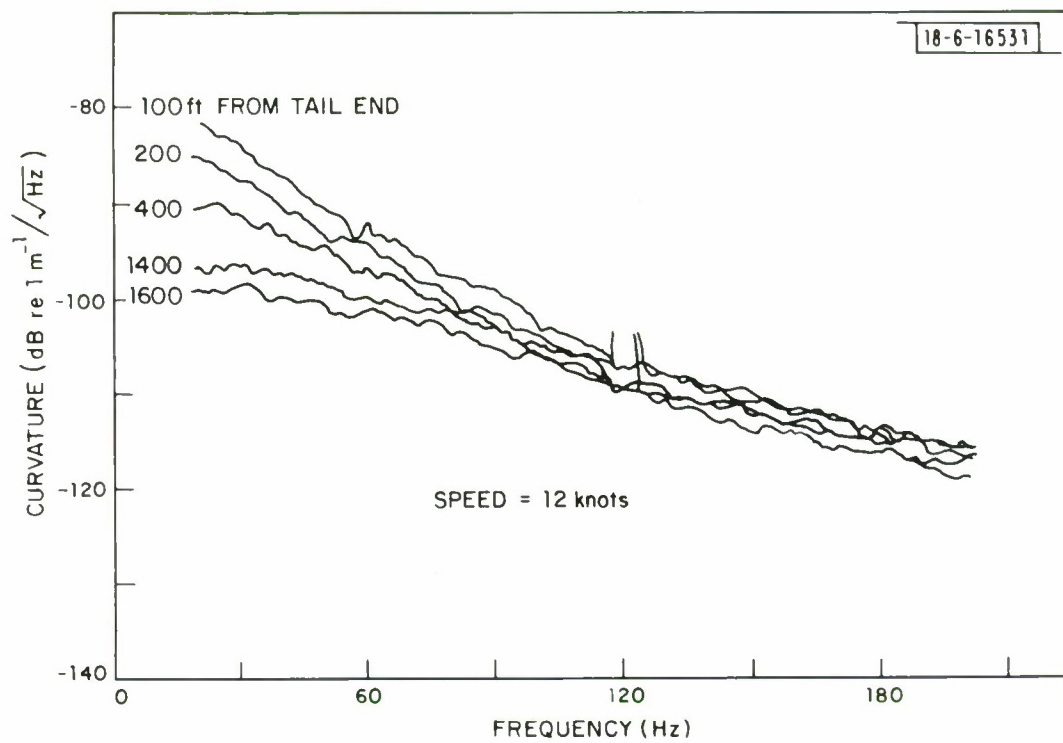


Fig. 18. Cable curvature spectra at five different gage-pair locations.

The spectra of longitudinal strain and of curvature measured during circular turns are shown in Figs. 19 and 20. If they are to be believed, they show that **at** the forward gage pair (i.e., near the submarine) both kinds of vibration can be some 40 dB or more higher in level than during a straight run. They are believable in the sense that this is true for at least one of the kinds of vibration. But since the data reduction procedure depends upon longitudinal strain being statistically independent of curvature, it may not be true for both. For a curved cable, the two are not independent and so the data reduction is suspect. It would not grossly magnify the apparent energy of both, but it could misapportion the energy between the two.

Near the tail end of the cable (400 ft. from the end, to be precise), the effect of the circular turn is not nearly as marked as it is near the tow point. In fact, Figs. 19 and 20 seem to show that, at the higher frequencies, the vibration levels are sometimes slightly less during circular turns than during straight runs.

The result of the circular turn tests is, therefore, that at low frequencies and near the tow point, a circular turn induces much higher vibration levels in the cable than does a straight run at the same speed. Whether the vibration spectra during turns are precisely as shown in Figs. 19 and 20 is in doubt, however, because the data reduction program may have misapportioned the total strain energy between the two kinds of vibration.

The purpose of the slow speed-increase test was to apply a slowly increasing tension to the cable and thereby cause the helically wound strength members on the cable slowly to unwind. This would then cause the cable at each

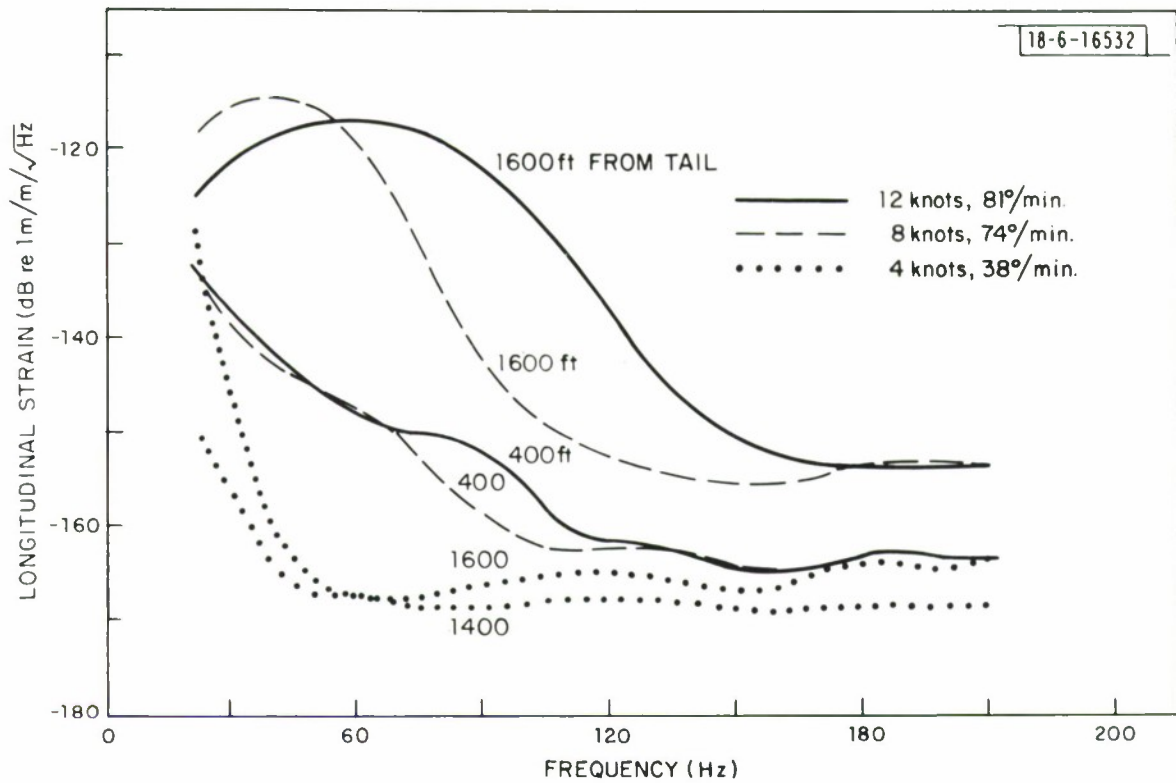


Fig. 19. Longitudinal strain spectra at different speeds during circular turns.

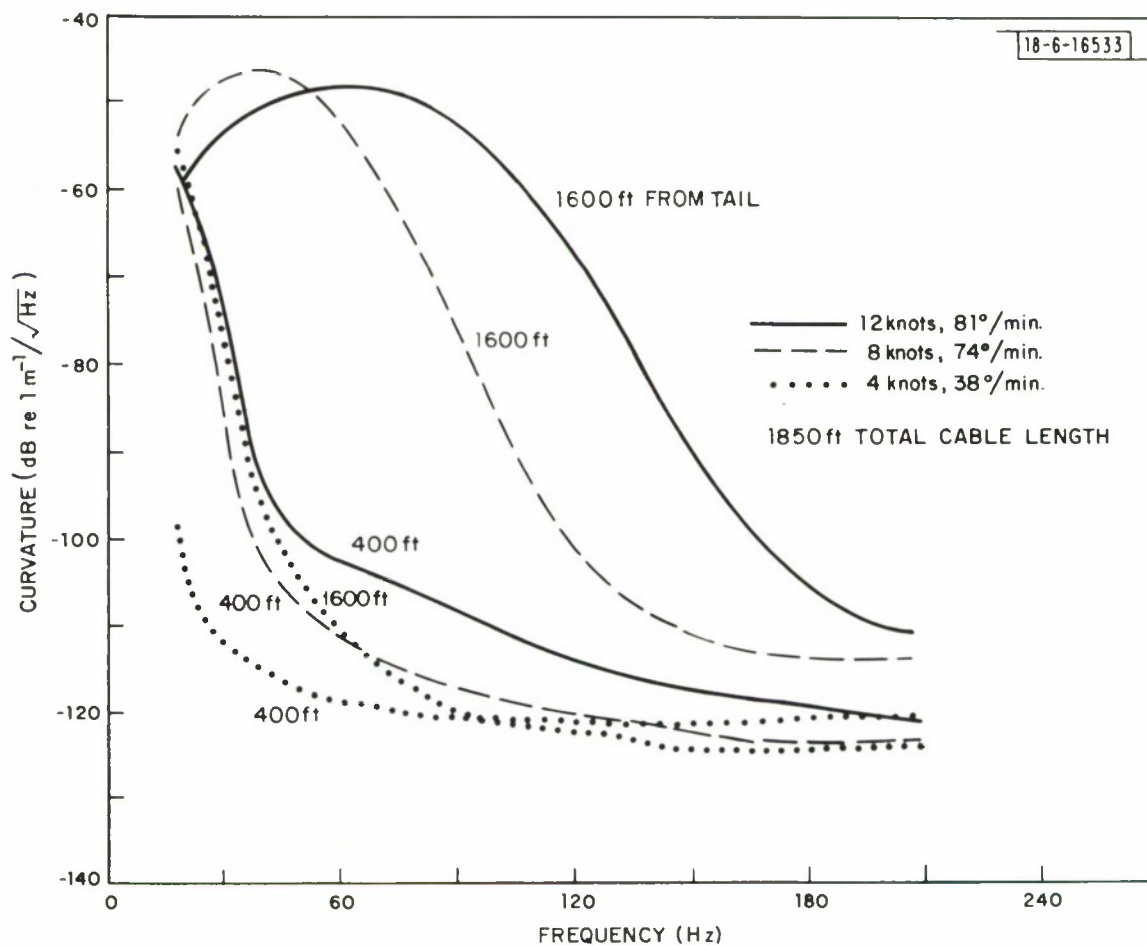


Fig. 20. Transverse curvature spectra at different speeds during circular turns.

gage location to revolve slowly about its longitudinal axis. Then, if at one moment a gage pair were registering the cable curvature in a vertical plane, some time later they would be registering the curvature in the horizontal plane. In this way, an azimuthal asymmetry in the transverse vibration of the cable would be observable as a cyclic variation in the mean square output voltage of the gages.

In fact, no such cyclic variation was observed. This could be explained by the proposition that the gage signal arising from cable curvature was much less than that arising from longitudinal cable strain, and so the curvature signal was unobservable to begin with. In fact, the reverse was the case. The gage signal arising from the cable curvature was at least 13 dB greater than that arising from the longitudinal strain. Thus it appears that the transverse vibration of the cable is statistically independent of the plane in which it is measured.

The last test to be carried out was an experiment to see if the three-wire gage connection used for all data runs was really necessary. It was used as a precaution against the possibility of the strain in the long connecting wires producing a spurious strain signal [6]. Figures 21 and 22 show the vibration spectra obtained using a two-wire gage connection with those obtained using the normal three-wire connection. The necessity for using the latter is clear. The error incurred in using a two-wire connection is seen to be more for the common mode longitudinal strain signal than for the differential mode curvature signal. This is to be expected, for the cable conductors all strain in unison and therefore tend to be self cancelling in the

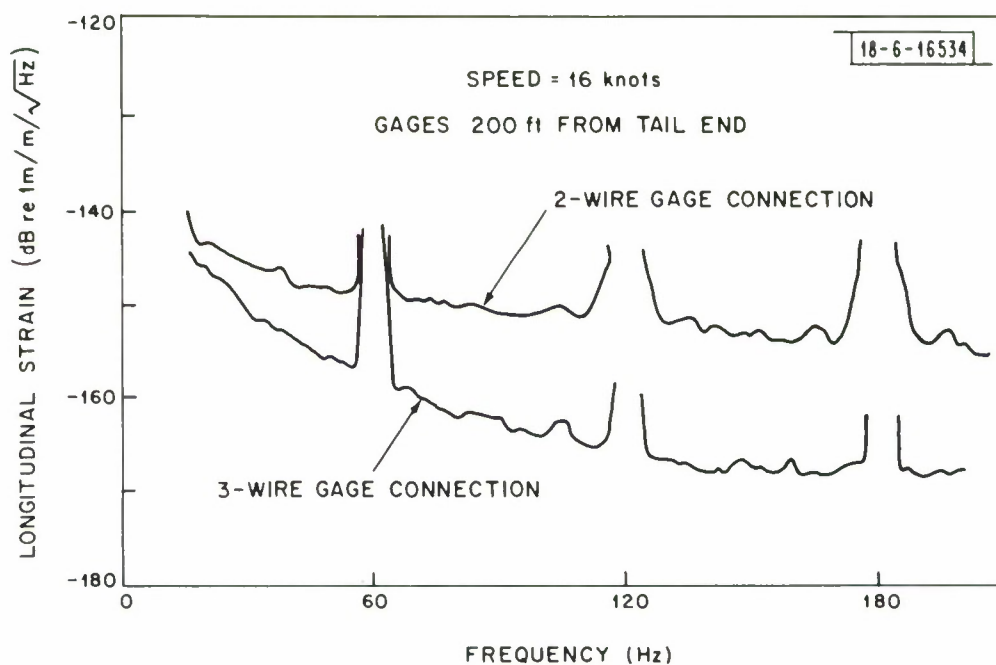


Fig. 21. Longitudinal strain spectrum measurement using a two-wire connection compared with that using the normal three-wire connection.

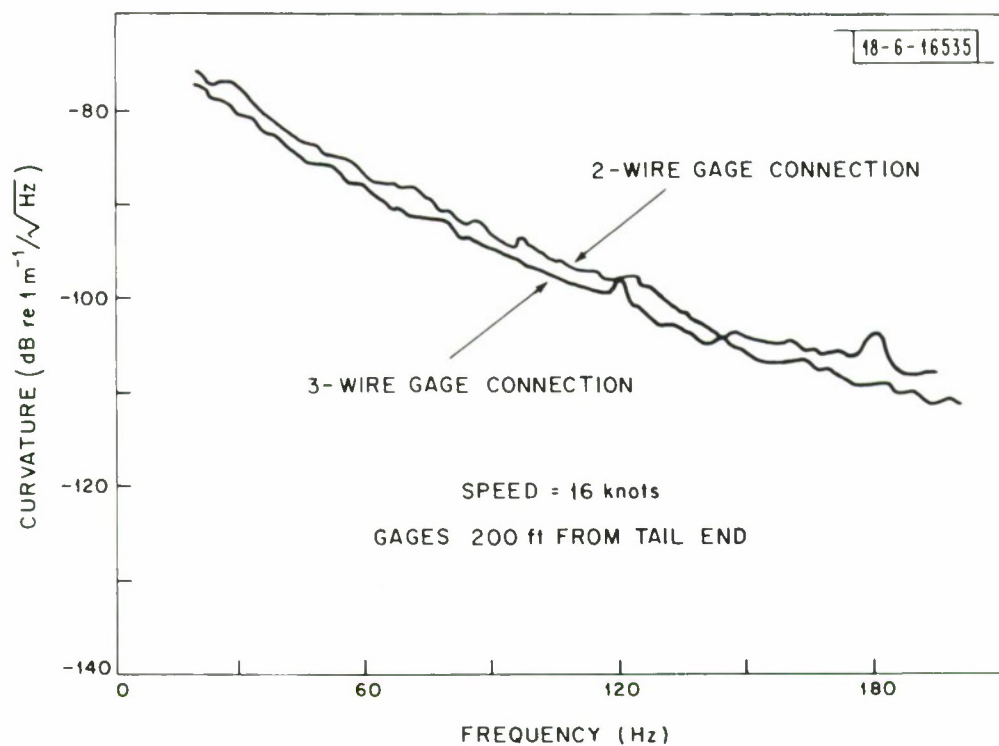


Fig. 22. Transverse curvature spectrum measurement using a two-wire gage connection compared with that using the normal three-wire connection.

error they cause in the strain difference.

The comments made earlier concerning the measured versus calculated gage calibration for longitudinal strain apply also to the calibration of the gages to cable curvature. The measured curvature calibration is -40 dB re. $1V/m^{-1}$, which is 6 dB less than the calculated calibration. Thus the spectra of curvature and derived motion-induced noise appearing in Fig. 13 of Ref. 2 should be raised by 6 dB.

IV. Derived Force Spectra

The smoothed average longitudinal strain spectra of Fig. 17 are seen to vary approximately as f^{-2} and v^{-4} , where v is the towing speed. But if $S_s(0, \omega)$ is the two dimensional power spectral density of the longitudinal shear force per unit length on the cable, then according to the local excitation model of cable vibration [2], the strain spectrum $S_\lambda(\omega)$ is given by

$$S_\lambda(\omega) = k_\ell^2 S_x(\omega) = \frac{k_\ell^3 Q_\ell}{\pi \omega^4 |m_\ell|^2} S_s(0, \omega) \quad (1)$$

Here Q_ℓ is the Q-factor of the cable vibration, k_ℓ is the longitudinal strain wave number and m_ℓ the effective mass per unit length for longitudinal vibration. All these parameters are defined in Ref. 2.

Since Q_ℓ is a weak function of frequency, and since k_ℓ is proportional to frequency, then to arrive at the result that $S_\lambda(\omega)$ is proportional to f^{-2} , it must be the case that $S_s(0, \omega)$ is proportional to f^{-1} . Therefore, to find a quantitative expression for the longitudinal shear force spectrum $S_s(0, \omega)$ which fits the measured cable strain it is appropriate to set

$$S_s(0, \omega) = \alpha \frac{v^4}{f} \quad (2)$$

and choose α so that the resulting strain, calculated using (1), is a good fit to the measured curves (Fig. 17).

To carry out the parameter fit it is necessary to know EA, the cable's longitudinal stiffness, in magnitude and phase, and also the specific density b of the cable. These were measured to be

$$\begin{aligned} EA &= 0.9 \times 10^6 (1 - i0.025) \text{ Newtons} \\ b &= 0.75. \end{aligned}$$

With a value of α of 9.0×10^{-9} MKS units, the strain spectra derived from the longitudinal shear force spectrum of Eq. (2) are shown plotted as solid lines in Fig. 23. The dashed lines are the experimentally measured smoothed average spectra shown in Fig. 17. It can be seen that the fit is reasonably good for practical purposes.

Thus, given the forcing function spectrum (2), one can calculate the resulting cable strain $S_\lambda(\omega)$ for any 0.65 inch diameter cable by simply measuring EA and b for the cable in question. The only other condition necessary for the validity of this derivation is that the surface of the cable should be hydrodynamically smooth [2]--a fairly benign requirement for the Reynolds numbers encountered in this application.

There is good reason to believe [7] that $S_s(0, \omega)$ is proportional to a^2 . If that is so, then the formula for it can be generalized further to

$$S_s(0, \omega) = 1.32 \times 10^{-4} \frac{v^4 a^2}{f}, \quad (3)$$

all units MKS. Then the strain spectrum in a cable of arbitrary diameter and mechanical properties can be calculated.

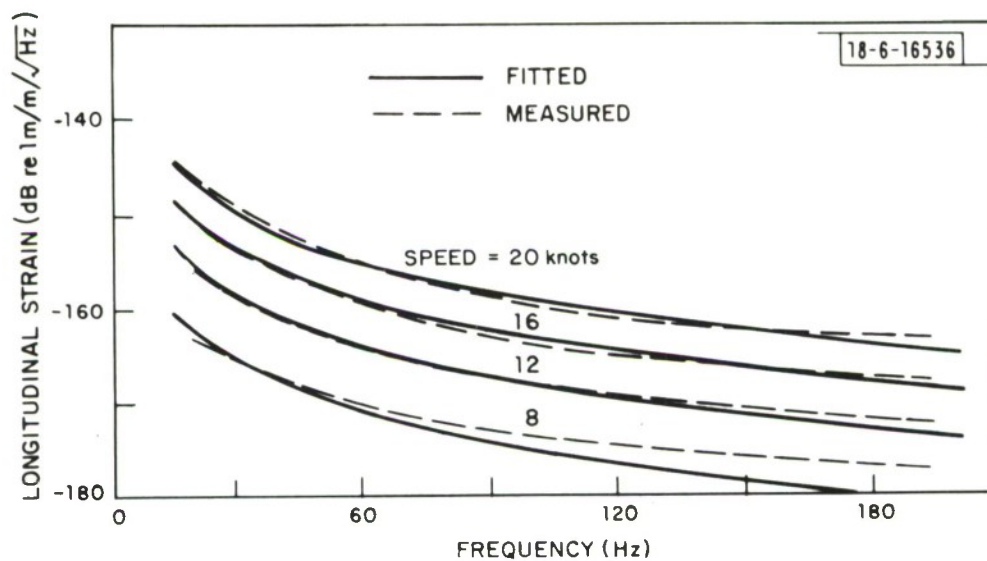


Fig. 23. Strain spectra calculated using the simple longitudinal shear force spectrum given in Eqs. (2) or (3) (solid curves) compared with smoothed average experimental curves (dashed curves).

For transverse cable vibration, the local excitation model [2] predicts that the curvature spectrum $S_c(\omega)$ is given by

$$S_c(\omega) = k_t^4 S_y(\omega) = \frac{k_t^5 Q_t}{\pi \omega^4 |m_t|^2} S_f(0, \omega). \quad (4)$$

Here k_t , Q_t and m_t are the wave number, Q-factor and effective vibrating mass associated with transverse cable vibration and $S_f(0, \omega)$ is the two dimensional power spectral density of the transverse force per unit length on the cable. From this equation, if $S_c(\omega)$ is known, then $S_f(0, \omega)$ can be calculated. The only extra data necessary are the buoyancy b and cable bending stiffness EI . From these, using the formulas of [2], k_t , Q_t and m_t can be calculated.

The cable bending stiffness EI was measured to be

$$EI = 1.2(1 \pm 10.12) \text{ Newton m}^2$$

and the buoyancy, as mentioned before, was measured to be 0.75. Using these values, the transverse force spectrum $S_f(0, \omega)$ corresponding to each measured curvature spectrum $S_c(\omega)$ was calculated. The result is the lightly drawn sets of spectra in Fig. 24.

There is a disturbingly large scatter in Fig. 24 in the different spectral density levels calculated for a particular frequency and speed. However, the derivation of $S_f(0, \omega)$ from $S_c(\omega)$ involved what may be an over simplified vibration model in which the bending stiffness is independent of tension and frequency and which requires that the tension be an accurately known function of speed.

Another, more direct, method of deriving $S_f(0, \omega)$ is by way of the electrode-pair antenna's measured noise voltage. If the noise voltage is motion-induced, then it is related to $S_f(0, \omega)$ by the following simple law [2]

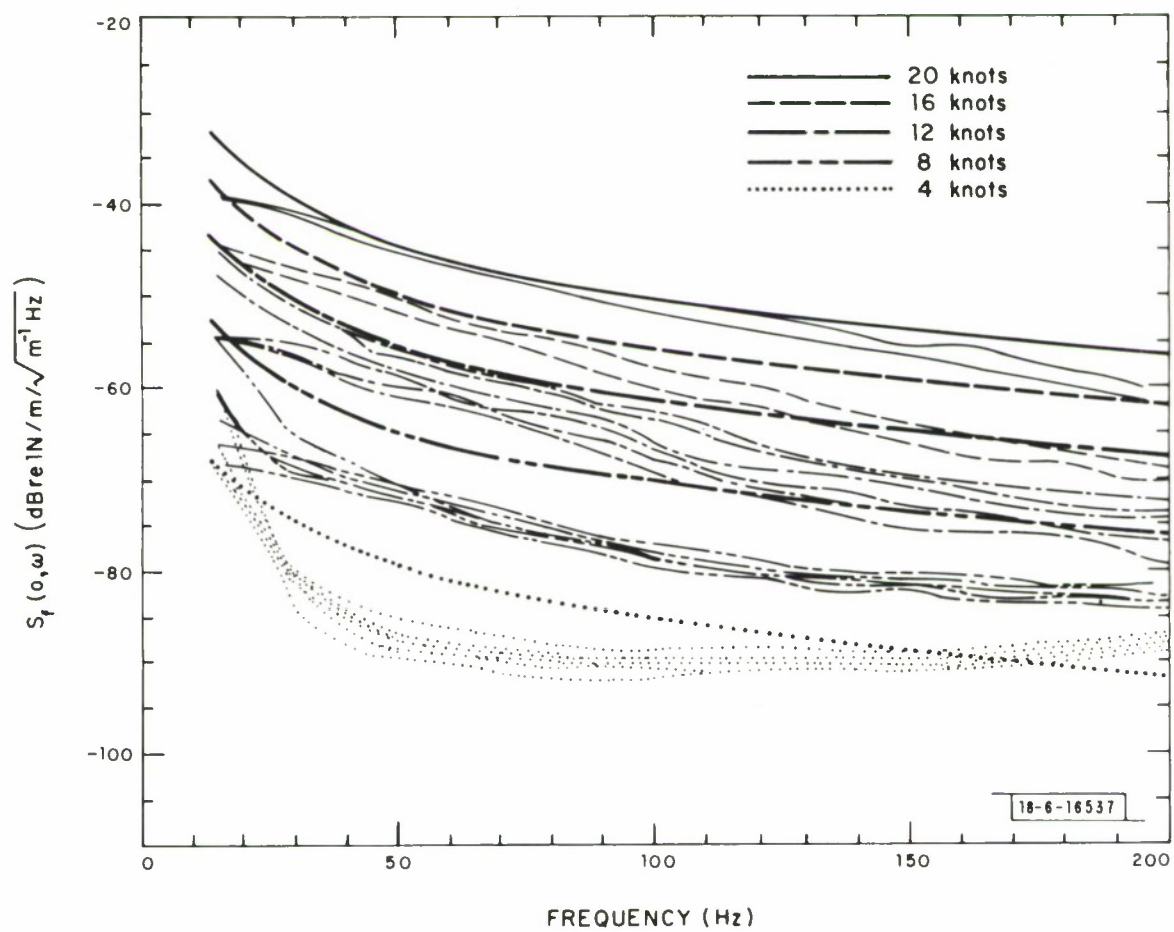


Fig. 24. Transverse force spectrum derived from strain gage curvature measurements (light curves) and from electrode pair noise voltage measurements (heavy curves).

$$S_v(\omega) = 2\ell \left(\frac{B_t}{\omega |m_t|} \right)^2 S_f(0, \omega). \quad (5)$$

Here 2ℓ is the length of the antenna, B_t the transverse component of the geomagnetic field and m_t the effective mass of the cable per unit length for transverse vibration. But the measured noise voltage in a 0.65 inch diameter, 300 m long electrode-pair antenna in a region where $B_t \approx 0.5 \times 10^{-4} T$ is very well represented as a function of frequency and speed by [3]

$$S_v(\omega) = 9.69 \times 10^{-14} \frac{v^5}{f^4}, \quad (6)$$

all units MKS. Thus, assuming the antenna cable's buoyancy was 0.75, one can invert (5) and (6) to obtain

$$S_f(0, \omega) = 7.16 \times 10^{-7} \frac{v^5}{f^2}, \quad (7)$$

all units MKS.

This spectrum is also plotted in Fig. 24 as the five heavily drawn curves.

Comparing the sets of lightly drawn curves in Fig. 24 with those heavily drawn, one sees that the total range as a function of speed is about the same for both sets and the general trend with frequency is much the same. Since the agreement is so marked, it must be the case that the electrode-pair antenna's dominant noise voltage is motion-induced and, since the law connecting its noise voltage with the transverse force spectrum is so simple, that the

force spectrum can be accurately derived from the electrode-pair antenna's noise voltage. That force spectrum is given by Eq. (7). It gives the fitted curves shown in Fig. 1, Ref. 3 when substituted in (5).

The deviations in Fig. 24 of the force spectra derived from the curvature measurements from the force spectra derived from electrode-pair measurements are therefore attributed to the uncertainties concerning cable tension, stiffness and damping as functions of speed and frequency. These are needed to derive force from curvature, but not to derive force from voltage.

Again, since $S_f(0,\omega)$ is, like $S_s(0,\omega)$, proportional [7] to a^2 , the force spectrum given by (7) can be generalized to

$$S_f(0,\omega) = 1.05 \times 10^{-2} \frac{v^5 a^2}{f^2} . \quad (8)$$

From this, and the properties of the cable, the curvature spectrum of an arbitrary cable towed at an arbitrary speed can be calculated.

V. Conclusions

The accelerometer and strain gage measurements have shown that the vibration of a cable towed behind a submarine is locally excited. That is, the vibration is excited by the fluctuating shear and pressure forces on the surface of the cable arising from the turbulent water flow in the boundary layer surrounding the cable. By fitting simple expressions for the shear and pressure force spectra to the measured data, quantitative formulas have been derived from which one can calculate the spectra of longitudinal strain and curvature for an arbitrary cable towed at an arbitrary speed. The only extra

data one needs are the mechanical properties and dimensions of the cable.

The answers to the questions raised in the Introduction are therefore that

i) The tail need be no longer than 100 feet, possibly could be even smaller. No vibration measurements were made closer than 100 ft. from the end of the cable, and so how closely within the last 100 ft. the statistically uniform vibration measured at other points approaches the tail end is not yet known.

ii) Since both longitudinal strain and curvature are locally generated, isolators would have marginal effect on the cable vibration in the antenna region.

iii) Since the cable's own turbulent boundary layer is the dominant source of the cable vibration, moving the antenna region further away from the submarine wake would have no effect.

iv) The quantitative agreement between the measured noise voltage of an electrode-pair antenna and its noise voltage calculated from the vibration measurements, strongly suggests that vibration, rather than hydromagnetic effects, is the source of the noise.

Acknowledgements

Many people have contributed to the work reported here. The accelerometer array and its instrumentation were put together by R. Jones of the Navy Underwater Systems Center, New London. All the data processing was expedited by T. Finnegan of the same Laboratory. Their agility and care in their respective fields made the whole experiment work properly. The strain gage cable and its electronics were built by O. G. Nackoney, H. J. Arbo, C. B. Swanton and D. P. Gale of Lincoln Laboratory. Their adaptability and creativity in novel technical directions repeatedly turned problem into achievement. Finally, recognition is due to O. G. Nackoney for going to sea and personally gathering the strain gage data.

APPENDIX A

STRAIN-GAGE PAIR DATA PROCESSING

If the amplifier gains were precisely their nominal values, and if the same were true for the gage sensitivities to curvature and to longitudinal strain, then the output voltages v_1 and v_2 of the two balanced gage channels would be given by

$$v_1 = v_\lambda + v_c \tag{A1}$$

$$v_2 = v_\lambda - v_c$$

where v_λ and v_c are the output voltages due to longitudinal strain and curvature separately. The gains may not be their nominal values, however, and the gage sensitivities can also be different. Thus the true situation can be represented by replacing Equations (A1) by

$$\begin{aligned} v_1 &= (\alpha v_\lambda + \beta v_c) e^{i\theta_1} \\ v_2 &= (\delta v_\lambda - \gamma v_c) e^{i\theta_2}, \end{aligned} \tag{A2}$$

where α , β , δ and γ are all real numbers close to unity to account both for the non-nominal gage sensitivities and for the non-nominal gain amplitudes, and θ_1 and θ_2 are real numbers to account for the non-nominal gain phases.

Since the sensitivity of each gage to cable curvature can vary independently of its sensitivity to longitudinal cable strain, β/α is not necessarily equal to γ/δ . Thus all four independent amplitude factors α , β , γ and δ are needed. The phase response of the amplifier affects both v_λ and v_c equally,

however, and so only two independent phase factors θ_1 and θ_2 are needed.

If α , β , δ , γ , θ_1 and θ_2 were known precisely, v_λ and v_c could be evaluated separately from any given pair of values of v_1 and v_2 by inverting (A2). Careful measurement could fairly readily establish θ_1 and θ_2 with sufficient accuracy, but an accurate measurement of the amplitude factors would require accurately known combinations of longitudinal strain and curvature to be established in the cable while each gage amplifier's output voltage was simultaneously being recorded. The mechanical problems involved in such a venture are formidable. There is incentive to seek an easier way.

Thus the measurement problem consists of estimating the separate power spectral densities $S_{\lambda\lambda}$ and S_{cc} of v_λ and v_c when only v_1 and v_2 are directly available, when the four amplitude factors are known only to the extent that they are close to unity and when the two phase factors are known to be small compared to a radian. The one crucial additional fact is that v_λ and v_c are statistically independent of one another-- $S_{\lambda c} \equiv 0$. This allows the separation of $S_{\lambda\lambda}$ and S_{cc} to be carried out, even though one might be much larger than the other.

Since the amplitude factors are close to unity, a measurement of the geometric mean quantities $\sqrt{\alpha\delta}v_\lambda$ and $\sqrt{\beta\gamma}v_c$ is essentially equivalent to a measurement of v_λ and v_c . Thus if these modified voltages be represented as v'_λ and v'_c , and then substituted into (A2), the result is

$$\begin{aligned} v_1 &= (av'_\lambda + bv'_c)e^{i\theta_1} \\ v_2 &= \left(\frac{1}{a}v'_\lambda - \frac{1}{b}v'_c\right)e^{i\theta_2} \end{aligned} \tag{A3}$$

where $a = \sqrt{\alpha/\delta'}$ and $b = \sqrt{\beta/\gamma'}$.

If b were equal to a , then since v'_λ and v'_c are statistically independent, the spectral density S_{11} of v_1 would be a^4 times the spectral density of S_{22} of v_2 . If, in addition, θ_1 and θ_2 were zero, the separate measurement of $S_{\lambda\lambda}$ and S_{cc} would then involve first computing the spectral densities S_{11} and S_{22} of v_1 and v_2 , evaluating the amplitude correction h by means of the formula $h^4 = S_{11}/S_{22}$, and then computing the spectral densities of $[(1/h)v_1 \pm hv_2]/2$. These last are equal to $S_{\lambda\lambda}$ and S_{cc} , respectively.

A procedure very similar to this can be used when $b \neq a$ and when θ_1 , $\theta_2 \neq 0$. The amplitude correction is calculated in the same way (and is therefore a compromise between the unequal correction factors needed to deal with the unequal amplitude factors a and b) and the phase correction is obtained by using the cross spectral density S_{12} (which is the expected value of $v_1 v_2^*$). The derivation of the procedure is as follows:

The correction factor h is given by

$$h^4 = \frac{S_{11}}{S_{22}} \quad (A4)$$

and, ideally, the phase differences between the channels should be corrected by modifying v_1 and v_2 by $e^{-i\theta_1}$ and $e^{-i\theta_2}$. That is, one computes the spectral densities

$$S_{\pm} = \left\langle \left| \frac{1}{2} \left(\frac{1}{h} v_1 e^{-i\theta_1} \pm h v_2 e^{-i\theta_2} \right) \right|^2 \right\rangle, \quad (A5)$$

where the angle brackets denote expected value. (It will transpire that θ_1

and θ_2 need not, in practice, be evaluated directly. See below.)

When (A4) is substituted in (A5) and the expected value of the sum of terms rewritten as the sum of the expected values of the terms, the result is

$$S_{\pm} = \frac{1}{2} [\sqrt{S_{11}S_{22}} \pm (S_{\lambda\lambda} - S_{cc})]. \quad (A6)$$

But since $S_{12} \equiv \langle v_1 v_2^* \rangle = (S_{\lambda\lambda} - S_{cc}) e^{i(\theta_1 - \theta_2)}$, and since θ_1 and θ_2 are assumed to be small compared with a radian, the term $S_{\lambda\lambda} - S_{cc}$ is equal to $\text{sgn}(\text{Re}\{S_{12}\}) |S_{12}|$. Therefore, (A6) can be rewritten as

$$S_{\pm} = \frac{1}{2} [\sqrt{S_{11}S_{22}} \pm \text{sgn}(\text{Re}\{S_{12}\}) |S_{12}|]. \quad (A7)$$

All the quantities in this expression can be computed from v_1 and v_2 . S_{11} and S_{22} are the auto spectra of v_1 and v_2 and S_{12} is the cross spectrum.

The question remaining is the extent to which S_{+} and S_{-} as defined by (A7) are estimates of $S_{\lambda\lambda}$ and S_{cc} .

By direct algebraic manipulation of (A3), it can be shown that

$$\sqrt{S_{11}S_{22}} = (S_{\lambda\lambda} + S_{cc}) \left\{ 1 + 4\xi \frac{S_{\lambda\lambda}S_{cc}}{(S_{\lambda\lambda} + S_{cc})^2} \right\}^{1/2}, \quad (A8)$$

where ξ is the "asymmetry factor"

$$\xi = \frac{1}{4} \left(\frac{a}{b} - \frac{b}{a} \right)^2. \quad (A9)$$

Therefore, by combining (A6) and (A8), and expressing the square root as the first two terms of its Taylor series, one obtains

$$\begin{aligned} S_+ &= S_{\lambda\lambda} \left(1 + \frac{S_{cc}}{S_{\lambda\lambda} + S_{cc}} \xi + O\{\xi^2\} \right) \\ S_- &= S_{cc} \left(1 + \frac{S_{\lambda\lambda}}{S_{\lambda\lambda} + S_{cc}} \xi + O\{\xi^2\} \right). \end{aligned} \tag{A10}$$

These expressions show that the sum and difference spectra S_+ and S_- , evaluated by means of the formula (A7), are closely equal to the required strain and curvature spectra $S_{\lambda\lambda}$ and S_{cc} . This remains true for both of them even when one is very large compared with the other. In fact, by examining the exact formulas for which (A10) are an approximation, one can show that in general

$$\begin{aligned} S_{\lambda\lambda} &\leq S_+ \leq (1+\xi)S_{\lambda\lambda} \\ S_{cc} &\leq S_- \leq (1+\xi)S_{cc} \end{aligned} \tag{A11}$$

If the unlikely event should occur that a/b is as far from its nominal value of unity as 1.5 (or 0.667), then $\xi = 0.17$, and in that case the maximum possible error in using S_+ and S_- as estimates of $S_{\lambda\lambda}$ and S_{cc} is 17 percent or 0.68 dB.

An example of the process is illustrated in Figs. A1 through A6. The first four show the two auto spectra $S_{11}(f)$ and $S_{22}(f)$ followed by the cross spectrum $S_{12}(f)$ in amplitude and phase. These spectra were taken using 1024 samples per second of the analog strain signals from gages 3 and 4 during a

16 knot straight run. The number of samples used for each Fourier transform was 512, which implies a resolution of 2 Hz. The mean square of a total of 128 such transforms comprised each auto spectrum. The cross spectrum was the mean of 128 cross products. As large a number as 128 transforms were averaged in order to get good estimates of $S_{11}(f)$, $S_{22}(f)$ and $S_{12}(f)$. Only then could a small longitudinal strain spectrum $S_{\lambda\lambda}(f)$ be accurately recovered in the presence of a large curvature signal $S_{cc}(f)$.

The result is shown in Figs. A5 and A6, which give, respectively, the sum spectrum $S_+(f)$ and difference spectrum $S_-(f)$.

Notable features present in the figures are:

i) The phase between the two strain signals (Fig. A4). It stands very close to 180° , except where perturbed by line frequency interference, across the whole band of frequencies. This indicates that the strain signals are dominated by the curvature signal, which, being a difference mode signal, is 180° removed in phase in one gage with respect to the other.

ii) The sum spectrum $S_+(f)$ (Fig. A5), which is the estimate of the longitudinal strain spectrum $S_{\lambda\lambda}(f)$, has a much lower level than the estimate $S_-(f)$ of the curvature spectrum $S_{cc}(f)$ (Fig. A6). This is consistent with the phase data of Fig. A4. Also, the sum spectrum $S_+(f)$ shows strong line frequency interference whereas the difference spectrum $S_-(f)$ does not. This would be expected, since line frequency interference is a common-mode phenomenon for identical gage connections to identical amplifiers. Particularly gratifying about the two figures, however, is that the separation between the two signal sources is so consistent. In places, the spectra differ by more than two orders of magnitude, and the computation of spectral levels is computed anew at every increment of 2 Hz. Nevertheless, the resulting spectra are smooth and distinct.

iii) The cross-spectrum amplitude, Fig. A3, is apparently indistinguishable from either of the auto spectra, Figs. A1 and A2, and yet the difference between them, in the form expressed by (A7), is not simply a random error. It is the sum spectrum $S_-(f)$ plotted in Fig. A5. (Since the phase of $S_{12}(f)$ is 180° , its real part has a negative sign.)

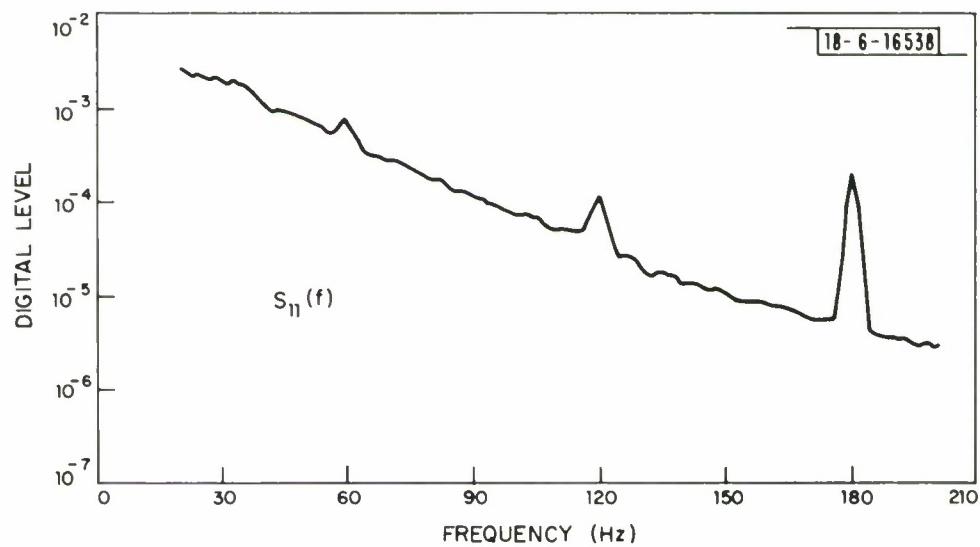


Fig. A1. The auto-spectrum of the strain signal from gage 3 at a speed of 16 knots and steady heading.

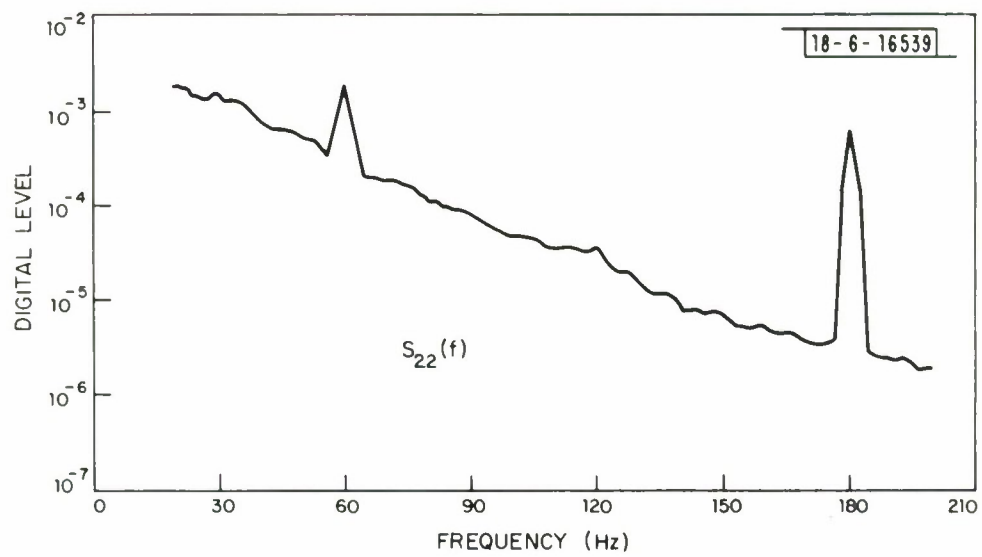


Fig. A2. The auto-spectrum of the strain signal from gage 4 at a speed of 16 knots and steady heading.

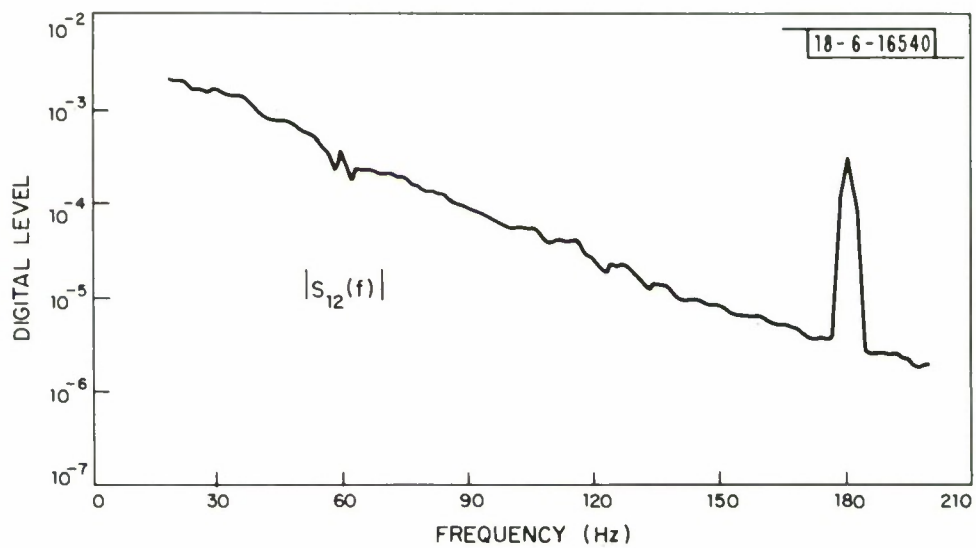


Fig. A3. The amplitude of the cross-spectrum of the strain signals from gages 3 and 4 at a speed of 16 knots and steady heading.

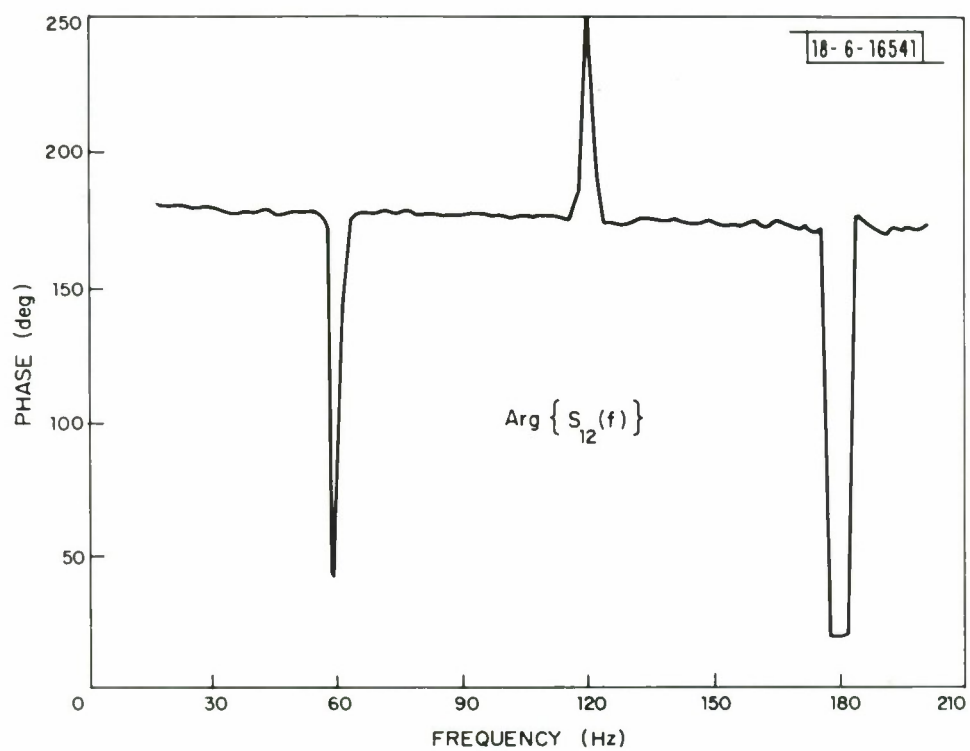


Fig. A4. The phase of the cross-spectrum of the strain signals from gages 3 and 4 at a speed of 16 knots and steady heading.

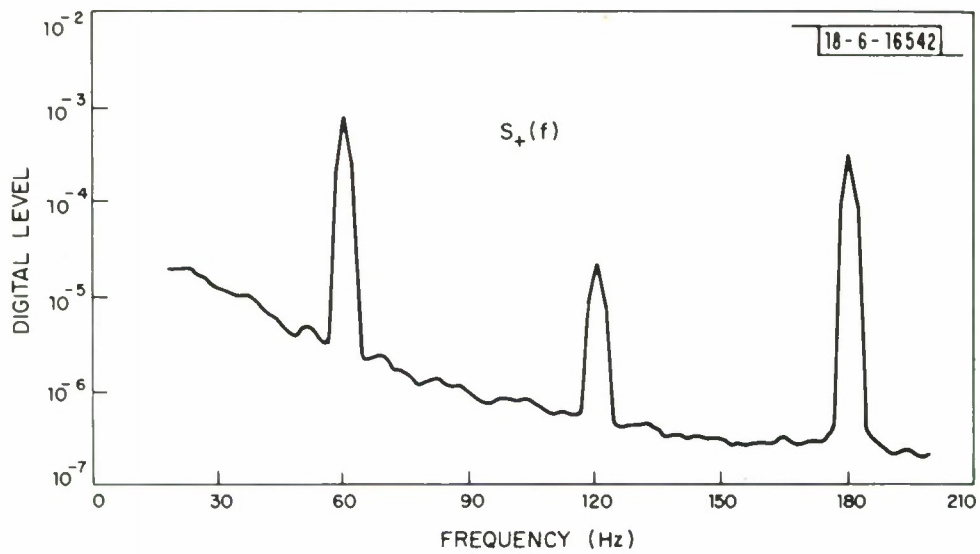


Fig. A5. The estimate of the longitudinal strain spectrum at the location of gages 3 and 4 at a speed of 16 knots and steady heading.

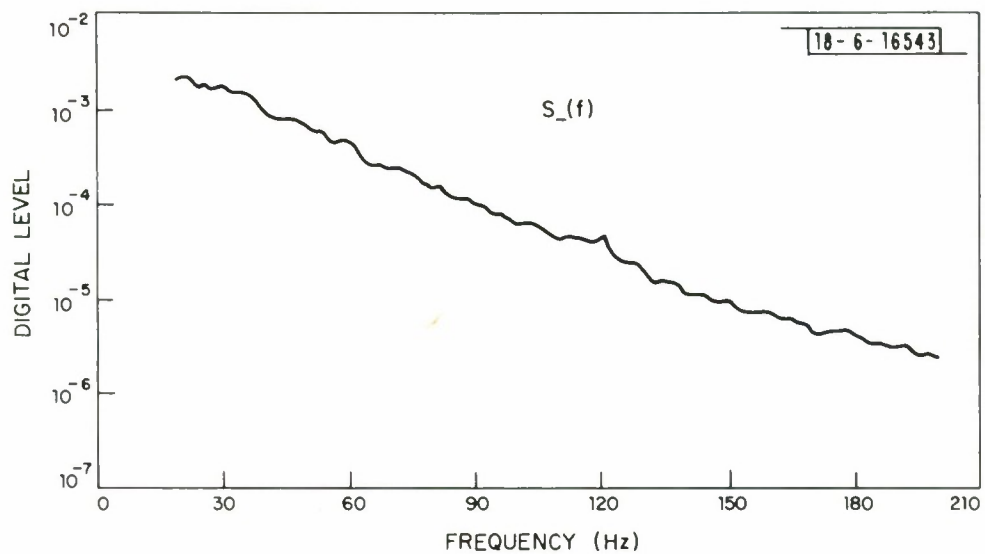


Fig. A6. The estimate of the curvature spectrum at the location of gages 3 and 4 at a speed of 16 knots and steady heading.

References

1. M. L. Burrows, "Motion-Induced Noise in Towed Flexible Sensors," Project Report NAC-15 (Navy Communications), Lincoln Laboratory, M.I.T. (24 March 1969), not generally available.
2. M. L. Burrows, "On the Design of a Towed ELF H-Field Antenna," Technical Note 1972-34, Lincoln Laboratory, M.I.T. (28 December 1972), DDC AD-754949.
3. M. L. Burrows, "Motion-Induced Noise in Electrode-Pair Extremely Low Frequency (ELF) Receiving Antennas," IEEE Trans. Commun. COM-22, No. 4, 540-542 (1974), DDC AD-A000458/0.
4. M. L. Burrows, "The Lincoln Submarine-Towed ELF Loop Antenna," Technical Note 1975-24, Lincoln Laboratory, M.I.T. (27 May 1975).
5. M. L. Burrows, "Performance of the ELF Antenna Water-Flow Tunnel," Technical Note 1975-19, Lincoln Laboratory, M.I.T. (27 May 1975).
6. O. G. Nackoney, "Strain Gage Instrumentation of a Buoyant Cable," Technical Note 1972-18, Lincoln Laboratory, M.I.T. (30 March 1972), DDC AD-744825.
7. M. L. Burrows, "Other Sources of Motion-Induced Noise in a Towed ELF H-Field Antenna," Technical Note 1973-21, Lincoln Laboratory, M.I.T. (25 May 1973), DDC AD-762936.

OUTSIDE DISTRIBUTION LIST

Chief of Naval Operations
Attn: Capt. W. Lynch (OP941P)
The Pentagon Department of the Navy
Washington, D.C. 20350

Chief of Naval Research (Code 418)
Attn: Dr. T. P. Quinn
800 North Quincy St.
Arlington, Va. 22217

Computer Sciences Corp.
Systems Division
Attn: Mr. D. Blumberg
6565 Arlington Blvd.
Falls Church, Va. 22046
(10 copies)

Director
Defense Communications Agency
Code 960
Washington, D.C. 20305

IIT Research Institute
Attn: Mr. A. Valentino, Div. E.
10 W. 35th Street
Chicago, Illinois 60616

Naval Civil Engineering Laboratory
Attn: Mr. J. R. Allgood
Port Hueneme, CA 93043

Naval Electronics Laboratory Center
Attn: Mr. R. O. Eastman
San Diego, CA 92152

Naval Electronic Systems Command
Attn: PME-117T, Mr. J. E. DonCarlos
Dept. of the Navy
Washington, D.C. 20360
(2 copies)

Naval Electronic Systems Command
Attn: PME-117-21, Capt. J. Galloway
Department of the Navy
Washington, D.C. 20360

Mr. George Downs
Strategic Systems, Electronic Sys. Gr.
GTE Sylvania, 189 B Street
Needham, Mass 02194

Naval Electronic Systems Command
Attn: PME-117-21A, Dr. B. Kruger
Department of the Navy
Washington, D.C. 20360

Naval Electronic Systems Command
Attn: PME-117-22, Cmdr. R. L. Gates
Department of the Navy
Washington, D.C. 20360

Naval Electronic Systems Command
Attn: PME-117-23,
Department of the Navy
Washington, D.C. 20360

Naval Electronic Systems Command
Attn: PME-117-24,
Leroy S. Woznak
Department of the Navy
Washington, D. C. 20360

Naval Facilities Engineering Command
Attn: Mr. G. Hall (Code 054B)
Washington, D.C. 20390

Naval Research Laboratory A
Attn: Mr. Garner
4555 Overlook Ave. S.W.
Washington, D.C. 20390

Naval Research Laboratory
Attn: Mr. R. LaFonde
4555 Overlook Ave. S.W.
Washington, D.C. 20390

New London Laboratory
Naval Underwater Systems Center
Attn: Mr. J. Merrill
New London, CT 06320
(4 copies)

The Defense Documentation Center
Attn: DDC-TCA
Cameron Station, Building 5
Alexandria, VA 22314

Naval Research Lab
Attn: Russel M. Brown, Code 5252
4555 Overlook Ave. S.W.
Washington, D. C. 20390

Dr. Philip Karr
Building M3 Room 2946
1 Space Park
Redondo Beach, CA 90278

Dr. A. C. Frazer-Smith
Radioscience Laboratory
Stanford University
Stanford, CA 94305

Dr. E. C. Field
Pacific Sierra Research Corp.
1456 Cloverfield Blvd.
Santa Monica, CA 90404

Capt. W. C. Cobb
Naval Electronic Systems Command
Attn: PME-117
Dept. of the Navy
Washington, D.C. 20360

UNCLASSIFIED

SECURITY CLASSIFICATION OF THIS PAGE (When Data Entered)

REPORT DOCUMENTATION PAGE		READ INSTRUCTIONS BEFORE COMPLETING FORM
1. REPORT NUMBER ESD-TR-75-177	2. GOVT ACCESSION NO.	3. RECIPIENT'S CATALOG NUMBER
4. TITLE (and Subtitle) Strain-Gage Vibration Measurements on a Submarine-Towed Antenna Cable		5. TYPE OF REPORT & PERIOD COVERED Technical Note
		6. PERFORMING ORG. REPORT NUMBER Technical Note 1975-22
7. AUTHOR(s) Burrows, Michael L.		8. CONTRACT OR GRANT NUMBER(s) F19628-73-C-0002
9. PERFORMING ORGANIZATION NAME AND ADDRESS Lincoln Laboratory, M.I.T. P.O. Box 73 Lexington, MA 02173		10. PROGRAM ELEMENT, PROJECT, TASK AREA & WORK UNIT NUMBERS Program Element 11403N Project No. 1511
11. CONTROLLING OFFICE NAME AND ADDRESS Naval Electronic Systems Command Department of the Navy Washington, DC 20360		12. REPORT DATE 27 May 1975
		13. NUMBER OF PAGES 64
14. MONITORING AGENCY NAME & ADDRESS (if different from Controlling Office) Electronic Systems Division Hanscom AFB Bedford, MA 01731		15. SECURITY CLASS. (of this report) Unclassified
		15a. DECLASSIFICATION/DOWNGRADING SCHEDULE
16. DISTRIBUTION STATEMENT (of this Report) Approved for public release; distribution unlimited.		
17. DISTRIBUTION STATEMENT (of the abstract entered in Block 20, if different from Report)		
18. SUPPLEMENTARY NOTES None		
19. KEY WORDS (Continue on reverse side if necessary and identify by block number) vibration measurements derived force spectra depressor accelerometer measurements cable vibration		
20. ABSTRACT (Continue on reverse side if necessary and identify by block number) As part of the developmental work on a submarine-towed ELF loop antenna, the mechanics of cable vibration have been studied analytically and cable vibration measurements with accelerometers and strain-gages have been carried out from surface vessels and from a submarine. The results are that both cable longitudinal strain and cable curvature, over the frequency range of 20 to 200 Hz, are excited by the fluctuating forces on the surface of the cable arising from the cable's own turbulent boundary layer. Neither vibration of the tow point nor the submarine wake are significant sources of mechanical energy. Generalized force spectra are derived from the measured vibration spectra. These then allow the levels of both types of vibration to be calculated for an arbitrary cable towed at an arbitrary speed.		

UNCLASSIFIED

SECURITY CLASSIFICATION OF THIS PAGE (When Data Entered)